ELSEVIER

Deep-Sea Research II 50 (2003) 3143–3169

DEEP-SEA RESEARCH
PART II

www.elsevier.com/locate/dsr2

Phytoplankton and iron: validation of a global three-dimensional ocean biogeochemical model

Watson W. Gregg[a,*], Paul Ginoux[b], Paul S. Schopf[c], Nancy W. Casey[d]

[a] *Laboratory for Hydrospheric Processes, NASA/Goddard Space Flight Center, Greenbelt, MD 20771, USA*
[b] *NOAA/Geophysical Fluid Dynamics Laboratory, Princeton, NJ 08542, USA*
[c] *Climate Dynamics Program, School for Computational Sciences, George Mason University, Fairfax, VA, USA*
[d] *Science Systems and Applications, Inc., 10210 Greenbelt Road, Suite 600, Seabrook, MD 20706, USA*

Received 25 April 2002; received in revised form 31 March 2003; accepted 15 July 2003

Abstract

The JGOFS program and NASA ocean-color satellites have provided a wealth of data that can be used to test and validate models of ocean biogeochemistry. A coupled three-dimensional general circulation, biogeochemical, and radiative model of the global oceans was validated using these in situ data sources and satellite data sets. Biogeochemical processes in the model were determined from the influences of circulation and turbulence dynamics, irradiance availability, and the interactions among four phytoplankton functional groups (diatoms, chlorophytes, cyanobacteria, and coccolithophores) and four nutrients (nitrate, ammonium, silica, and dissolved iron).

Annual mean log-transformed dissolved iron concentrations in the model were statistically positively correlated on basin scale with observations ($P<0.05$) over the eight (out of 12) major oceanographic basins where data were available. The model tended to overestimate in situ observations, except in the Antarctic where a large underestimate occurred. Inadequate scavenging and excessive remineralization and/or regeneration were possible reasons for the overestimation.

Basin scale model chlorophyll seasonal distributions were positively correlated with SeaWiFS chlorophyll in each of the 12 oceanographic basins ($P<0.05$). The global mean difference was 3.9% (model higher than SeaWiFS).

The four phytoplankton groups were initialized as homogeneous and equal distributions throughout the model domain. After 26 years of simulation, they arrived at reasonable distributions throughout the global oceans: diatoms predominated high latitudes, coastal, and equatorial upwelling areas, cyanobacteria predominated the mid-ocean gyres, and chlorophytes and coccolithophores represented transitional assemblages. Seasonal patterns exhibited a range of relative responses: from a seasonal succession in the North Atlantic with coccolithophores replacing diatoms as the dominant group in mid-summer, to successional patterns with cyanobacteria replacing diatoms in mid-summer in the central North Pacific. Diatoms were associated with regions where nutrient availability was high. Cyanobacteria predominated in quiescent regions with low nutrients.

While the overall patterns of phytoplankton functional group distributions exhibited broad qualitative agreement with in situ data, quantitative comparisons were mixed. Three of the four phytoplankton groups exhibited statistically significant correspondence across basins. Diatoms did not. Some basins exhibited excellent correspondence, while most showed moderate agreement, with two functional groups in agreement with data and the other two in disagreement.

*Corresponding author. Tel.: +1-301-614-5711; fax: +1-301-614-5644.
E-mail address: watson.gregg@nasa.gov (W.W. Gregg).

0967-0645/$ - see front matter
doi:10.1016/j.dsr2.2003.07.013

The results are encouraging for a first attempt at simulating functional groups in a global coupled three-dimensional model but many issues remain.

1. Introduction

Modeling distributions of global biogeochemical constituents in the oceans is an important step toward synthesizing data collection activities in the context of the JGOFS effort. The extensive data sets produced by the project, in addition to satellite data sets produced by NASA ocean color missions, together can provide a basis for further understanding the processes involved in producing biogeochemical distributions, and serve as a test bed for models that attempt to synthesize these processes in a forward, i.e., predictive manner. Many processes remain poorly understood despite a decade of in situ observations, and so disparities between model results based on these observations and the observations themselves can yield clues as to the causes.

In a previous paper (Gregg, 2002a), a coupled physical/biogeochemical/radiative model was developed and used to understand and characterize the nature and causes of interannual variability of phytoplankton and nutrients during the Sea-Viewing Wide Field-of-view Sensor (SeaWiFS) era (1997–2000). In this effort, we attempt to expand the model to explicitly include iron biogeochemistry. Also in this effort, we introduce a biogeochemically important fourth phytoplankton functional group, coccolithophores, to the overall phytoplankton mix. The purpose of this paper is to utilize the in situ observations provided mostly by the JGOFS effort and satellite data to validate a global, coupled three-dimensional model including iron biogeochemistry and multiple phytoplankton groups, in order to diagnose its performance. In this manner, we may begin to address shortcomings in our knowledge and assumptions, by taking into account the global ocean biogeochemical scenario as a whole.

2. Methods

Briefly, the model is a coupled general circulation/biogeochemical/radiative three-dimensional model of the global oceans. It spans the domain from -84° to 72° latitude in increments of 1.25° longitude by $2/3^\circ$ latitude. A full description can be found in Gregg (2000, 2002a). The model has been modified to include full iron biogeochemical cycling and growth limitation, and to introduce a fourth phytoplankton functional group, coccolithophores, in addition to diatoms, chlorophytes (which are intended to represent prasinophytes, pelagophytes, and other nanoflagellates), and cyanobacteria (which are intended to represent all pico-prokaryotes) (Fig. 1). Another minor addition is a second detrital component, to separate detrital processes associated with diatoms (which include silica), and those associated with

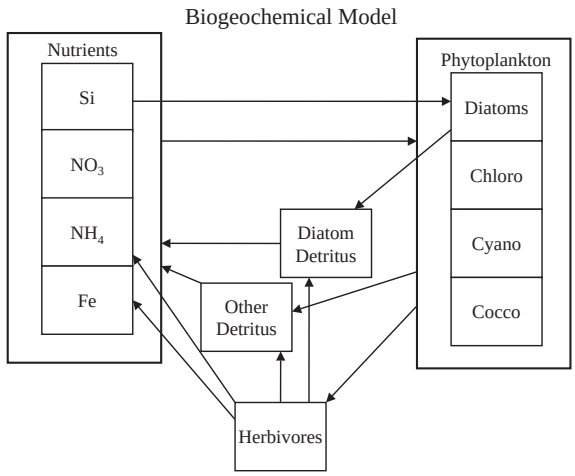

Fig. 1. Diagrammatic representation of the biogeochemical model. Four phytoplankton components (diatoms, chlorophytes, cyanobacteria, and coccolithophores) interact with four nutrient components (nitrate, ammonium, silica, and iron), and contribute to detritus when ingested or upon death, which returns to the ammonium pool immediately and the nitrate, silica, and iron pools later upon remineralization. Herbivores ingest phytoplankton groups non-preferentially, and contribute to the ammonium and iron pools through excretion, and eventually the nutrient pools upon death and remineralization. Two detrital pools represent one deriving from diatoms and another deriving from other phytoplankton.

the other groups (which do not). These modifications are described mathematically in Appendix A.

2.1. Iron biogeochemistry

It is now well established that iron limitation plays an important role in phytoplankton dynamics, at least in some parts of the ocean (Coale et al., 1998; Kolber et al., 1994; Martin et al., 1990). A realistic model of the global oceans must include iron biogeochemical dynamics to provide a comprehensive representation of ocean biogeochemistry. Unlike macro-nutrients like nitrogen and silica, a large proportion of the oceanic dissolved iron derives from the atmosphere, usually associated with soil dust transported as aerosols.

2.1.1. Atmospheric iron deposition

In this model we utilize the dust deposition fields calculated with the Georgia Institute of Technology/Goddard Global Ozone Chemistry Aerosol Radiation and Transport (GOCART) model (Ginoux et al., 2001). The GOCART model is driven by assimilated meteorology from the Goddard Earth Observatory System-Data Assimilation System (GEOS-DAS). The dust sources in GOCART have been identified globally from satellite data (Prospero et al., 2002), and dust is entrained into the atmosphere according to surface conditions, namely soil moisture and friction velocity.

Four dust size fractions are transported, corresponding to clay (smallest) and three increasing fractions of silt. The dust is transported via atmospheric circulation processes and falls to the oceans as both dry deposition (particle settling) and wet deposition (associated with rainfall). The dust deposition amounts used here are climatological mean values over the period 1982–2000, except for 1997, 1998, and 1999, for which simulations are unavailable. We assumed that the iron content varied among the clay and silt fractions as follows: clay = 3.5% iron, silt = 1.2% iron (Fung et al., 2000). We further assumed that iron solubility was 1% for all fractions, which represents the low end of current estimates (Fung et al., 2000). We recognize that a constant solubility is probably unrealistic, due to differences in dust particle sizes, iron source, and local presence/absence of organic substances in seawater, among others. However, quantitative information on how iron solubility is affected by these and other influences is not currently available, and consequently we have chosen a single rate, following the lead of other explicit iron biogeochemical models to date (e.g., Moore et al., 2002; Christian et al., 2002; Archer and Johnson, 2000; Leonard et al., 1999).

2.1.2. Iron/phytoplankton growth limitation

It is also well established that iron limits the growth of ocean phytoplankton differently among phytoplankton functional groups. Diatoms have been shown to exhibit the greatest sensitivity to iron limitation (Price et al., 1994; Miller et al., 1991a; Morel et al., 1991a,b). We used the diatom half-saturation constant (0.12 nM) from Fitzwater et al. (1996), a value also used by Leonard et al. (1999) in an iron-limitation model study in the Equatorial Pacific (Fig. 2). Coccolithophores have been shown to exhibit the lowest sensitivity in intercomparative laboratory studies (Sunda and Huntsman, 1995; Brand, 1991). Using the observations of Sunda and Huntsman (1995), we derived a half-saturation constant (k_F) for coccolithophores equal to 0.67 that of diatoms (Fig. 2; Appendix A). Chlorophytes have also been shown to exhibit iron limitation (Vassiliev et al., 1995), although intercomparison studies are not available. We set their half-saturation constants midway between the coccolithophores and diatoms, i.e., 0.835 times the diatom k_F (Fig. 2). Cyanobacteria are more difficult to characterize. Price et al. (1994) evaluated a picoplankton-dominated phytoplankton community in the mesotrophic (chlorophyll = 0.3 mg m^{-3}) tropical Pacific and derived a half-saturation constant of 0.034 nM, about one-fourth the diatom-dominated community rate measured by Fitzwater et al. (1996). However, measurements by Price et al. (1994) at an oligotrophic station (chlorophyll = 0.07 mg m^{-3}) in the North Central Pacific produced $k_F = 0.22$ nM. Oligotrophic waters are nearly always dominated by picoplankton (see Results). Carefully-controlled intercomparative

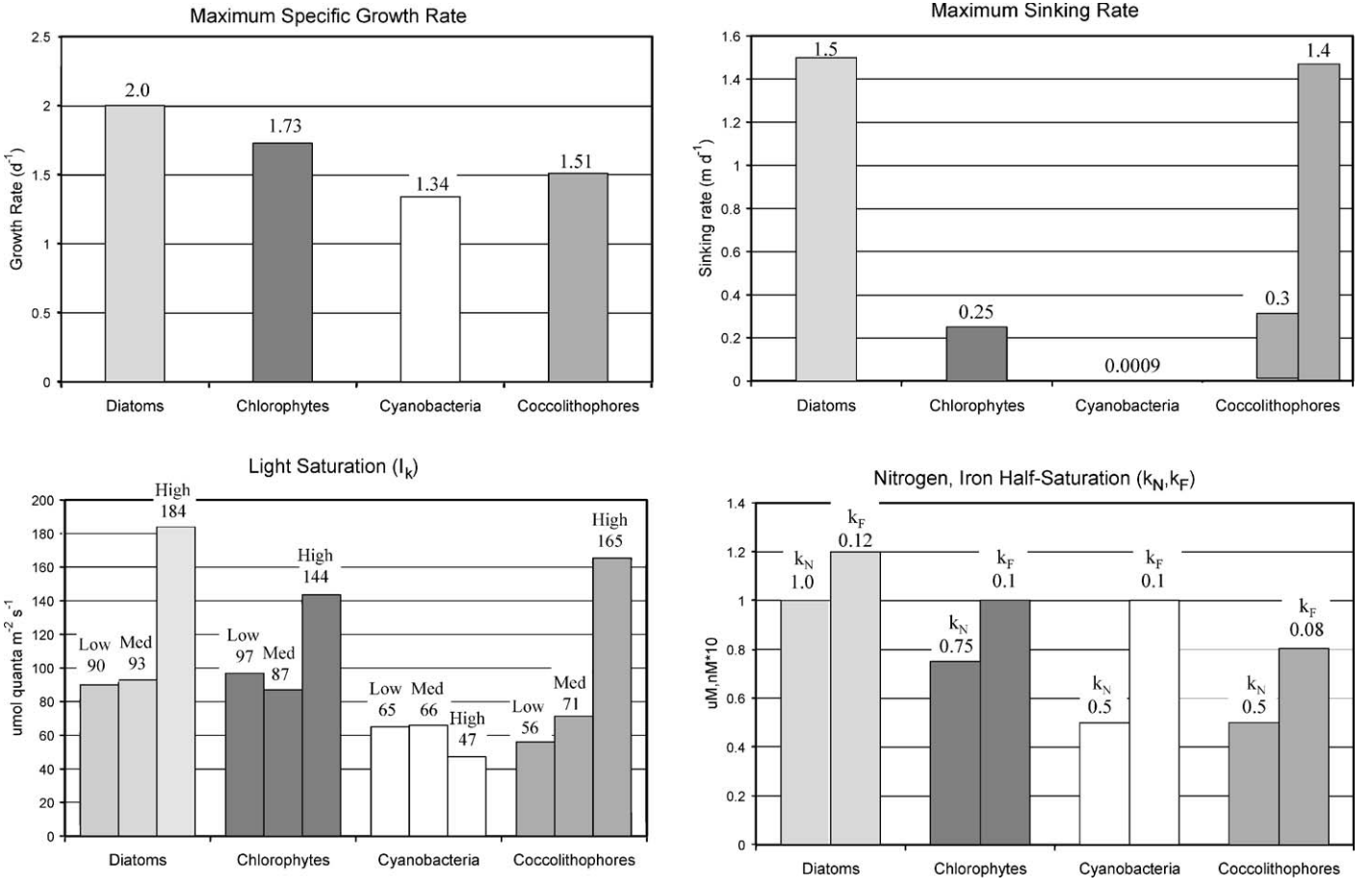

Fig. 2. Phytoplankton group physiological and physical characteristics. Top left: maximum specific growth rate (d^{-1}) at 30°C. Top right: Sinking rate (m d^{-1}). Bottom left: Light saturation parameters, I_k. Low light is defined as <50 μmol quanta m^{-2} s^{-1}, medium light is 50–200, and high light is >200. Bottom right: half-saturation constants for nitrogen (k_N) and iron (k_F). These figures illustrate the biological variety incorporated in the coupled model.

laboratory studies by Brand (1991) and Brand et al. (1983) indicated that cyanobacteria (*Synechococcus* spp.) susceptibility to iron limitation was nearly equal to that of diatoms. Mann and Chisholm (2000) also found evidence of iron limitation by cyanobacteria (*Prochlorococcus* sp.). These results are somewhat conflicting, and may be indicative of cyanobacterial diversity in oceanic environments. Several ecotypes of *Prochlorococcus* and *Synechococcus* spp. have been suggested by Mackey et al. (2002). We set the half-saturation constants of cyanobacteria midway between the coccolithophores and diatoms (Fig. 2), as a compromise among the observations and studies. However, we also found that setting k_F of cyanobacteria equal to that of coccolithophores produced negligible change in the phytoplankton distributions in the model.

The carbon:iron ratio is set at 150,000 (mol:mol), which represents an intermediate value of net and nanoplankton by Leonard et al. (1999). No differences among phytoplankton groups were enforced.

2.1.3. Iron recycling

Iron is assumed to remineralize from the detrital pool at the same rate as nitrate, and regenerate upon grazing and death the same as ammonium. Scavenging of dissolved iron was evaluated at $5.0\text{E} \times 10^{-5}$ d^{-1}. This represents about twice the rate used by Moore et al. (2002), excluding an exponential increase occurring at dissolved iron concentrations > 0.6 nM.

2.2. Coccolithophore characterization

As with the other phytoplankton functional groups, physiological, physical, and optical characterization of coccolithophores was obtained by reference to carefully controlled inter-comparative laboratory studies. For the physiological characterization, we require growth rates, half-saturation constants for nitrogen, and light saturation values. Growth rates (Fig. 2) were determined from Brand et al. (1983, 1986), Falkowski et al. (1985), Gavis et al. (1981), and Eppley et al. (1969). The coccolithophore half-saturation constant for nitrogen (k_N) was observed by Eppley et al. (1969) to be one-half the value of diatoms. Given this k_N for coccolithophores, new k_N's for chlorophytes and cyanobacteria were developed. Cyanobacteria k_N was set equal to the coccolithophores, assuming small particle size leads to improved nutrient uptake efficiency (Fig. 2). Chlorophyte k_N was set midway between diatoms and coccolithophores. Light saturation values were derived from Perry et al. (1981) for haptophytes, and represented values in three photoadaptation states. These states corresponded to the laboratory measurements, and were implemented in the model as low, medium, and high light intensities, as well as for the other three groups (Fig. 2, Appendix A).

Coccolithophore sinking rates (Fig. 2) were allowed to vary as a function of growth rate from 0.3 to 1.4 m d^{-1} based on observations by Fritz and Balch (1996). A linear relationship was assumed

$$w_s(\text{coc}) = 0.752\ \mu_m(\text{coc}) + 0.225, \quad (1)$$

where w_s is the sinking rate of coccolithophores (m d^{-1}), and μ_m is the maximum growth rate actually achieved. The calculation is performed once per day. Optical properties of coccolithophores were derived from several laboratory studies and are beyond the scope of the present paper. Their values and references can be found in Gregg (2002b).

2.3. Comparison of model with data sets

2.3.1. Iron

A survey of the published literature enabled the creation of a comprehensive data set of dissolved iron concentrations containing 1951 total observations at various depths. The observations were scattered among the global oceans and contained almost no repeat samples representing seasonal variability. In our analysis of model performance against these data, we first averaged the observations over the surface mixed layer as computed from the model for the location and month of the observation. We gathered all co-located observations and model results into annual means, since seasonal trends were not available, within the 12 major oceanographic basins of the global oceans

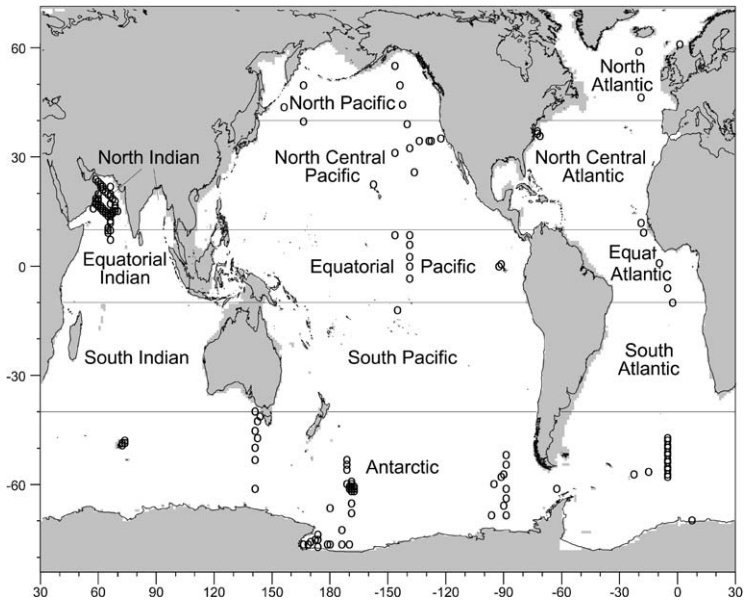

Fig. 3. Location of samples of dissolved iron indicated in the model domain, in which the 12 major oceanographic basins of the global oceans are identified. The annotated and fully referenced data set is available on anonymous ftp at salmo.gsfc.nasa.gov, at /pub/outgoing/modeldata. References from which the data set was derived are: Bowie et al. (2002), Boyd et al. (2000), Bucciarelli et al. (2001), Coale et al. (1996), de Baar et al. (1995, 1999), DiTullio et al. (1993), Gledhill et al. (1998), Gordon et al. (1998), Hall and Safi (2001), Loscher et al. (1997), Johnson et al. (1997, 2001), Martin and Gordon (1988), Martin et al. (1989, 1990, 1993), Measures and Vink (1999, 2001), Nakabayashi et al. (2001), Rue and Bruland (1995, 1997), Sedwick et al. (1999, 2000), Takeda et al. (1995), Tappin et al. (1995), Timmermans et al. (2001), Wu and Luther (1996).

(Fig. 3). The annual means represented co-located data and model points (to the nearest model grid point), and provided information on model performance within these basins. Not all basins were represented by the in situ database. We excluded observations in the eastern Equatorial Pacific that occurred during an El Niño. Chavez et al. (1999) showed that nitrate concentrations decreased two orders of magnitude in the tropical Pacific during the 1997–1998 El Niño, and similar effects may be expected with respect to iron. North Sea observations by Gledhill et al. (1998) were extremely high compared to others, which may indicate contamination or possibly anomalous conditions here, and also were eliminated from the analysis. Data were log-transformed because of the wide range of values in the global oceans (span a range of two orders of magnitude).

2.3.2. Chlorophyll

SeaWiFS data were obtained from the NASA/Goddard Earth Sciences (GES)-DAAC. Version 4 Level-3 monthly mean SeaWiFS chlorophyll data were re-gridded from the native 4096×2048 grid (approximately 10 km) onto the model grid for the period Sep 1997 through Jun 2002.

2.3.3. Phytoplankton functional groups

Phytoplankton functional group data is even more scarce than iron. Historically, phytoplankton function group distributions were anecdotal and qualitative, but they have been adequate to give us an overall understanding of large scale distributions. We have surveyed the published literature and obtained 359 surface layer observations of phytoplankton group abundances (Fig. 4). They have been converted when necessary into percent abundance of the entire population to compare to the model. We have made no distinction between abundances expressed as carbon and those expressed as chlorophyll, since no reliable data on carbon:chlorophyll ratios are available for functional groups. With the advent of high-performance liquid chromatography (HPLC,

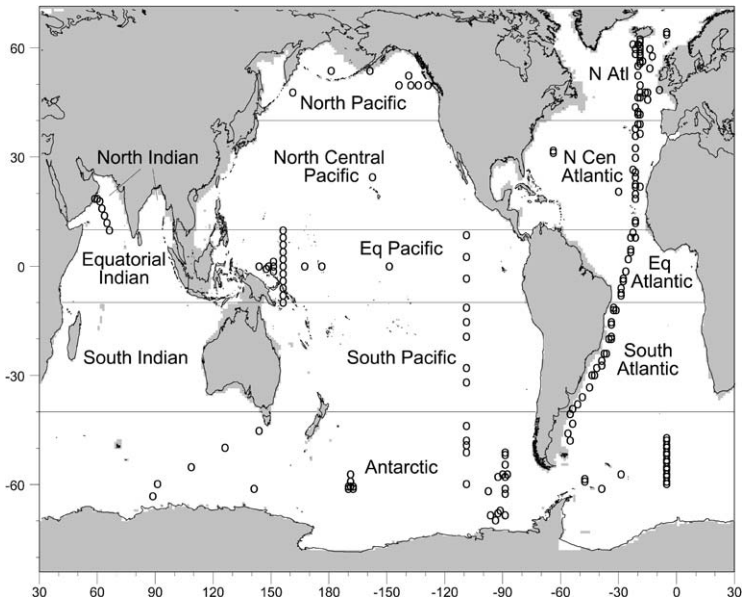

Fig. 4. Location of samples of phytoplankton functional group relative abundances indicated in the model domain. The locations denote where any functional group relative abundance was reported. The annotated and fully referenced data set is available on anonymous ftp at salmo.gsfc.nasa.gov, at /pub/outgoing/modeldata.

e.g., Bidigare et al., 1989), there has been a recent explosion of phytoplankton group information. Most HPLC investigations identify a broad class of Prymnesiophytes, but do not distinguish between *Phaeocystis* spp. and coccolithophores, since the pigment composition is similar. Functionally (ecologically, biogeochemically, and optically), these two groups are quite different. We believe *Phaeocystis* spp. falls more appropriately into the chlorophyte/nanoflagellate functional class in our model. Therefore, unless a reported distinction is made in the investigation, we are unable to use Prymnesiophyte data, since they represent an unknown proportion of *Phaeocystis* spp. (which we classify under chlorophytes) and coccolithophores. Both the chlorophyte/flagellate and coccolithophore observations must be neglected in these instances. This occurred fairly frequently in our data set. An exception was in the low latitudes, where we assumed all Prymnesiophytes to be coccolithophores, due to prevalent observations of coccolithophores being present and even abundant in these latitudes, while observations of *Phaeocystis* spp. suggest a limited occurrence.

We investigated satellite observations to help with identification of coccolithophore abundances, but no such product is available yet from the GES-DAAC. The Moderate Resolution Imaging Spectroradiometer Project has plans for producing coccolith and calcite distribution products, but validated data are not yet available. Brown and Yoder (1994) and Iglesias-Rodriguez et al. (2002) estimated coccolithophore distributions from coccoliths (essentially representing elevated water-leaving radiance at 555 nm) derived from the Coastal Zone Color Scanner and SeaWiFS, respectively, but also were not validated against in situ data.

In our analysis of the phytoplankton group data, we match up model mixed layer relative abundances with the location and month of the in situ observations. As with iron, we average the co-located, coincident model and data over the basin annually. This provides us an opportunity to observe the large scale spatial performance

of the model while keeping a close model-data relationship.

2.4. Model initialization

The model was initialized with annual climatologies for nitrate and silica from Conkright et al. (1994). Initial dissolved iron concentrations were taken from Fung et al. (2000), with a bottom boundary condition of 0.6 nM. The bottom boundary condition corresponds to suggestions by Archer and Johnson (2000) and to the mean of 11 observations $\geqslant$2000 m by Martin et al. (1989, 1993) and Coale et al. (1996). The remaining biological/chemical variables were set to constant values: 0.5 μM ammonium, and 0.05 mg m^{-3} for each of the phytoplankton groups. The model was integrated for 20 years using climatological monthly mean forcing from the National Center for Environmental Prediction Reanalysis products, and then integrated an additional six years with interpolated climatological daily mean forcing. Forcing fields include wind stress, shortwave radiation, sea-surface temperature, salinity, ice concentrations, and surface spectral irradiance (Gregg, 2002a). All analyses in this paper are for the 26th year of simulation.

3. Results and discussion

3.1. Comparison of dissolved iron with in situ data

Annual mean model log-transformed dissolved iron concentrations were positively correlated on basin scale with observations ($P<0.05$) over the eight basins for which in situ data were available (Fig. 5). The correlation coefficient (r) was 0.86 with a coefficient of determination (r^2) of 0.74. The slope was near 1 at 0.97 with a small y-intercept of 0.03. Low concentrations were simulated in the North and North Central Pacific, North Atlantic, and Antarctic, and high values in the North and Equatorial Indian and the North Central Atlantic. These simulations generally corresponded to the observations. The low concentrations in the North Atlantic were obtained in May and June, when uptake was very high compared to input.

The overestimations by the model may be caused by inadequate scavenging in the model, excessive regeneration or remineralization, and/or

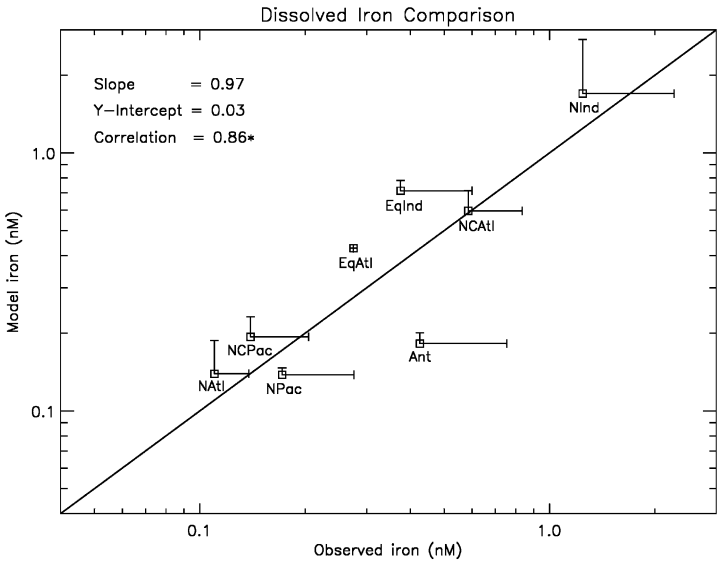

Fig. 5. Dissolved iron comparison of model vs. data. Shown are annual means of co-located, coincident model and data values by oceanographic basin. Error bars indicate the standard deviation: horizontal for data and vertical for model. The relationship between model and observed dissolved iron is statistically significant ($P<0.05$). Statistics on the relationship are shown in the figure.

slow detrital sinking rate. In the Southern Ocean, where a substantial underestimate occurred, large variability exists in observations from different investigators, which are difficult to reconcile since the observations were in different locations and seasons.

Seasonal distributions of model dissolved iron concentrations are shown in Fig. 6. Areas of high iron concentration are located near areas of high dust input, such as the Equatorial and North Central Atlantic, Equatorial and North Indian Ocean, and the northern portion of the South Indian. Low concentrations are apparent in the South Pacific central gyre region and the southernmost portions of the Antarctic. Seasonal reductions appear in the North Atlantic and eastern North Pacific. Relatively small meridional variability is observed in the Antarctic. Moderate values are observed in the Equatorial Pacific. Other investigations of global iron distributions by Moore et al. (2002) and Archer and Johnson (2000) produced lower estimates here in conformance with observations. Moore et al. (2002) did not include horizontal transport and the simulations were the result of atmospheric deposition, biological uptake and export, and boundary conditions strictly located at the one-dimensional points in the eastern Pacific. Our simulated higher concentrations do not derive directly from atmospheric deposition either, but are the result of

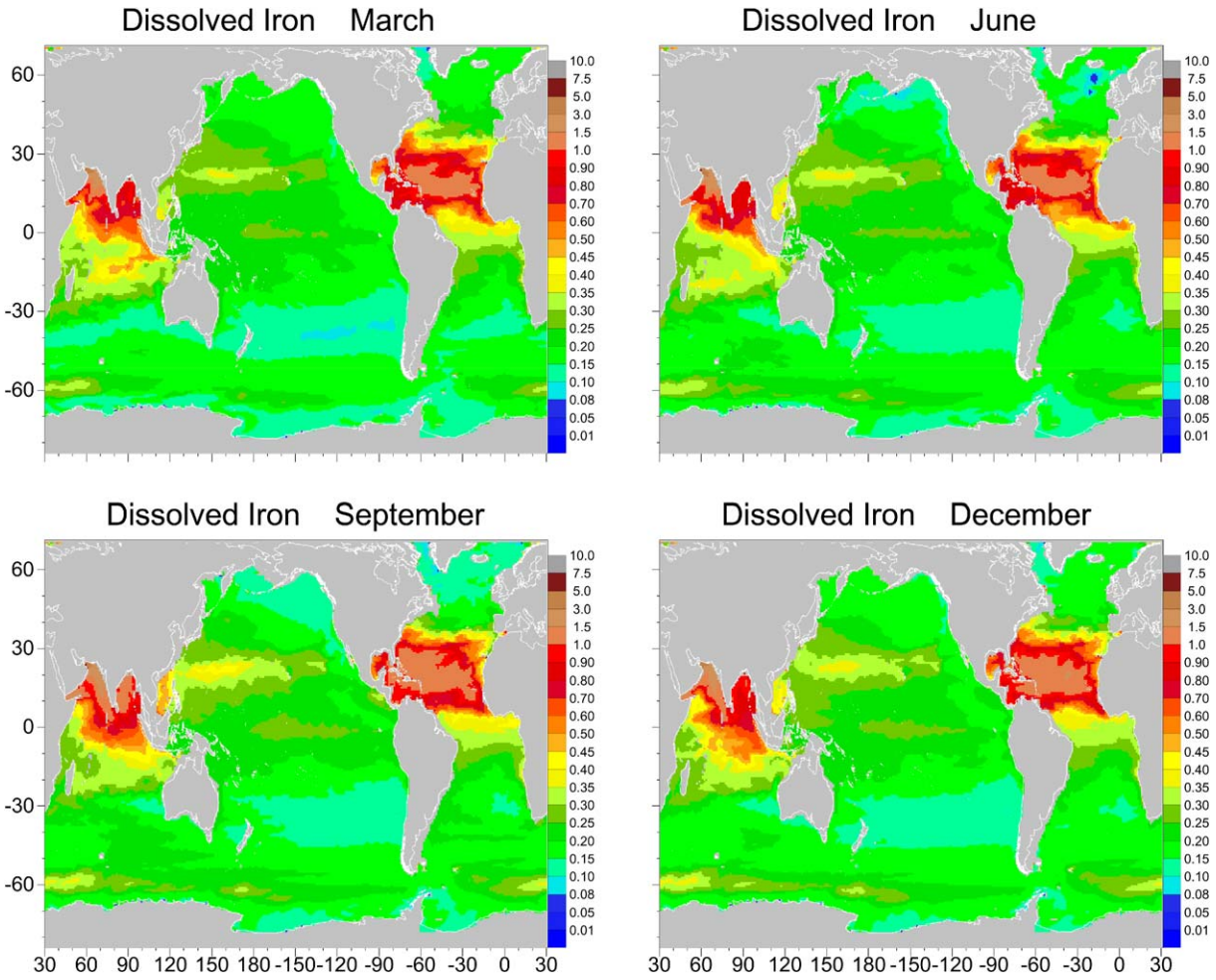

Fig. 6. Distribution of dissolved iron (nM) in the model for four months: March, June, September, and December.

atmospheric deposition on the western portion of the basin and eastward transport with the equatorial undercurrent, and subsequent upwelling along the equator and coast in the east, that developed in the course of our 26-year run. Archer and Johnson (2000) achieved their best results in an implicit biology simulation using a maximum scavenging function. Our higher values are most likely the result of excessive upwelling in the Equatorial Pacific, with contributions from possibly inadequate sinking and scavenging losses, and perhaps excessive remineralization/regeneration. Excessive upwelling is a common problem in coarse-to-medium resolution models (Oschlies, 2000), and nitrate values are also higher than observed here (Gregg, 2000). Solution of this problem requires increased spatial resolution or higher order numerical advection procedures (e.g., Oschlies and Garcon, 1999).

There remain serious issues related to the accuracy and precision of in situ dissolved iron measurements (Measures and Vink, 2001). Our data base of iron observations contains no repeat sampling in the same season and location by different investigators, so there is little basis for forming conclusions on methodologies. Thus a rigorous, point-by-point comparison of model results and observations is not practical at this time. We have chosen in our analysis to use annual means in oceanographic basins for our comparisons, to try to minimize these methodological effects. The comparisons should be interpreted in a broad context, as indicative of general basin-scale trends.

From the model perspective, the main effects of inclusion of iron limitation compared to earlier results (Gregg, 2002a) were (1) reduced total chlorophyll in the North Pacific by 10–20%, (2) reduction of diatom relative abundances by about 30% in the Equatorial Pacific, and (3) reduced total chlorophyll in the Antarctic by about 15%. These regions represent High Chlorophyll-Low Nutrient regions of the oceans, where iron limitation is expected to occur.

3.2. Comparison of chlorophyll with SeaWiFS

Seasonal total chlorophyll concentrations from the model agree quite well with SeaWiFS observations at the basin scale (Fig. 7). Correlation analysis shows that statistical significance is achieved seasonally between the model and SeaWiFS in every oceanographic basin ($P<0.05$, Fig. 7). An exception is the tropical Pacific but this basin exhibits almost no seasonal variability in SeaWiFS chlorophyll as a basin mean, which is properly indicated by the model, and so this is an artifact of correlation analysis. There is actually substantial agreement between the model and SeaWiFS here as seen in Fig. 7.

The North Indian Ocean exhibits statistically significant correlation between the model and SeaWiFS, however, the SeaWiFS August mean chlorophyll value for this region is about 8 times larger than the model. The SeaWiFS mean chlorophyll, at 1.3 mg m^{-3}, represents the largest monthly mean value in the SeaWiFS record. The disagreement is partly due to absorbing aerosols that bias the SeaWiFS algorithms and produce anomalously high chlorophyll estimates (Moulin et al., 2001). Even taking this into account, the model estimates are still most likely low here, as in situ observations also indicate higher concentrations than the model. In situ records during the southwest monsoon (Conkright et al., 1998) range from about 0.3 to 0.7 mg m^{-3} in the Arabian Sea, which is less than SeaWiFS but still greater than the model range of about 0.15 to 0.45 mg m^{-3}.

The global annual mean difference between SeaWiFS and the model is 3.9%. Considering basin-scale means, no region ever exceeds 90% difference for any season. The largest model underestimates occur in the North Indian Ocean, which is often 50–75% larger in SeaWiFS than in the model. The overestimation of dissolved iron in the tropical Pacific does not appear to have important effects on total chlorophyll concentrations, as the model tends to be lower than SeaWiFS here by an annual mean of 2.5%. However, this does not mean iron limitation is not occurring here, as phytoplankton group distributions are affected, as described earlier.

Imagery of simulated chlorophyll shows that generally, large-scale features are represented in the model and conform to SeaWiFS data: vast areas of low chlorophyll in the mid-ocean gyres, elevated chlorophyll in the equatorial and coastal

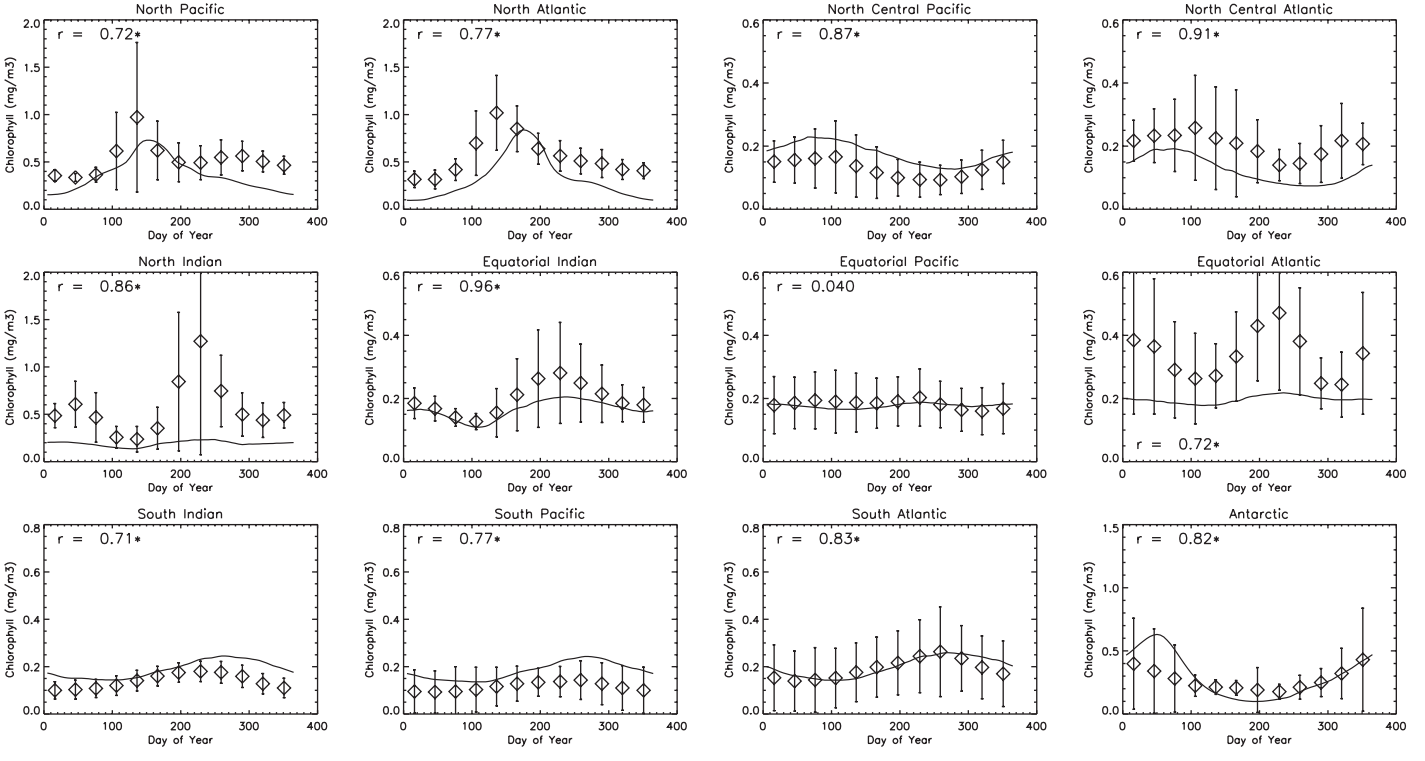

Fig. 7. Comparison of model-generated mean chlorophyll (solid line) with climatological monthly mean SeaWiFS chlorophyll (open diamonds) for the 12 major oceanographic basins in the global oceans. Error bars on the SeaWiFS chlorophyll represent one-half the SeaWiFS standard deviation. The correlation coefficient is indicated. An asterisk indicates that the correlation is significantly positively correlated ($P<0.05$). The probability value to establish statistical significance is 0.576. The equatorial Pacific does not indicate positive correlation because of the lack of seasonal variability in either result. However, this lack of seasonal variability in both the model and SeaWiFS indicates agreement.

upwelling regions, and large concentrations in the sub-polar regions (Fig. 8). The large scale features of the seasonal variability are represented as well: blooms of chlorophyll in local spring/summer (June) in the high latitudes, followed by retreat in the local winter (January), expansion of low chlorophyll regions associated with the central gyres in local summer, followed by contraction in winter.

January represents a period when phytoplankton growth in the Southern Hemisphere is reaching its peak and growth in the Northern Hemisphere is minimal (Fig. 8). Relatively low chlorophyll concentrations exist north of about 50°N with bands of moderate chlorophyll at the sub-polar convergence zone. The Southern Hemisphere bloom is apparent in SeaWiFS imagery, especially in the Atlantic sector of the Antarctic, with a large bloom apparent offshore of the Patagonian shelf. Other major plumes appear just north of the Ross Sea, and in the central part of the Indian sector. These features are generally represented by the model, but the meridional variability in SeaWiFS is much larger.

In June the Northern Hemisphere spring bloom is in full swing in SeaWiFS imagery, and is apparent in the model (Fig. 8). The northerly extent of the bloom extends to the edge of the model domain in the SeaWiFS imagery, and nearly so in the model. There is more spatial

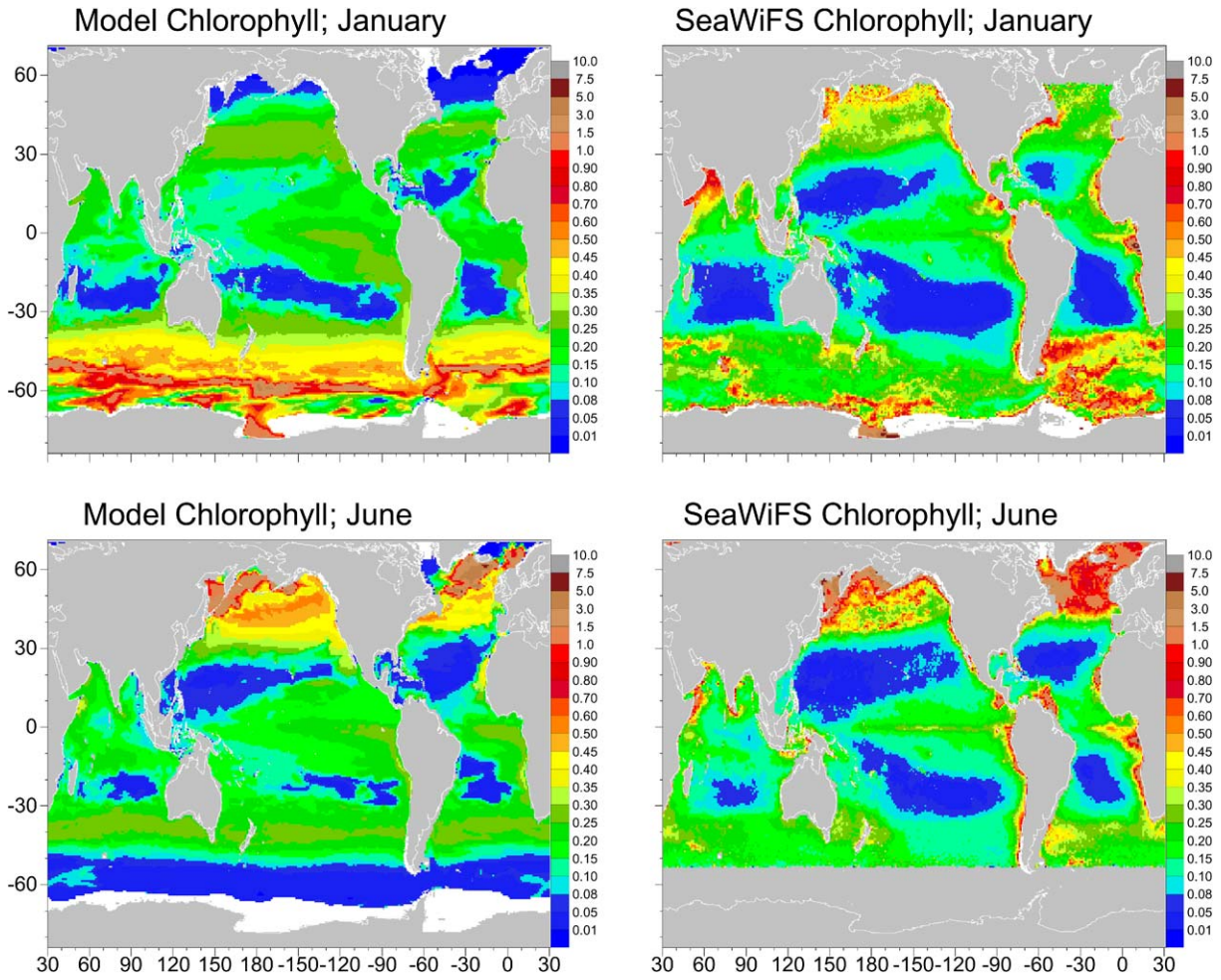

Fig. 8. Comparison of model and SeaWiFS chlorophyll for January and June. Ice fields are shown as white. Units are mg m^{-3}.

variability in the North Pacific in the SeaWiFS than in the model, but magnitudes and extent are similar. While there are many specific features of the North Atlantic bloom that differ between model and SeaWiFS, the overall structure and magnitude is similar.

3.3. Phytoplankton group distributions

Phytoplankton group distributions were initialized as equal and homogeneous concentrations throughout the model domain both horizontally and vertically. In June after 26 years of simulation, the four phytoplankton functional groups arrived at distributions that generally conform to expectations: diatoms inhabit high latitudes (except the North Pacific), coastal, and equatorial upwelling regions; cyanobacteria are abundant the central ocean gyres; and chlorophytes inhabit transitional regions (Fig. 9). Coccolithophores are abundant in the North Atlantic south of Iceland in June. High concentrations have been observed here in several observational studies (e.g., Boyd et al., 1997; Robertson et al., 1994; Holligan et al., 1993) and in satellite data analyses (Iglesias-Rodriguez et al., 2002; Brown and Yoder, 1994). Diatom and

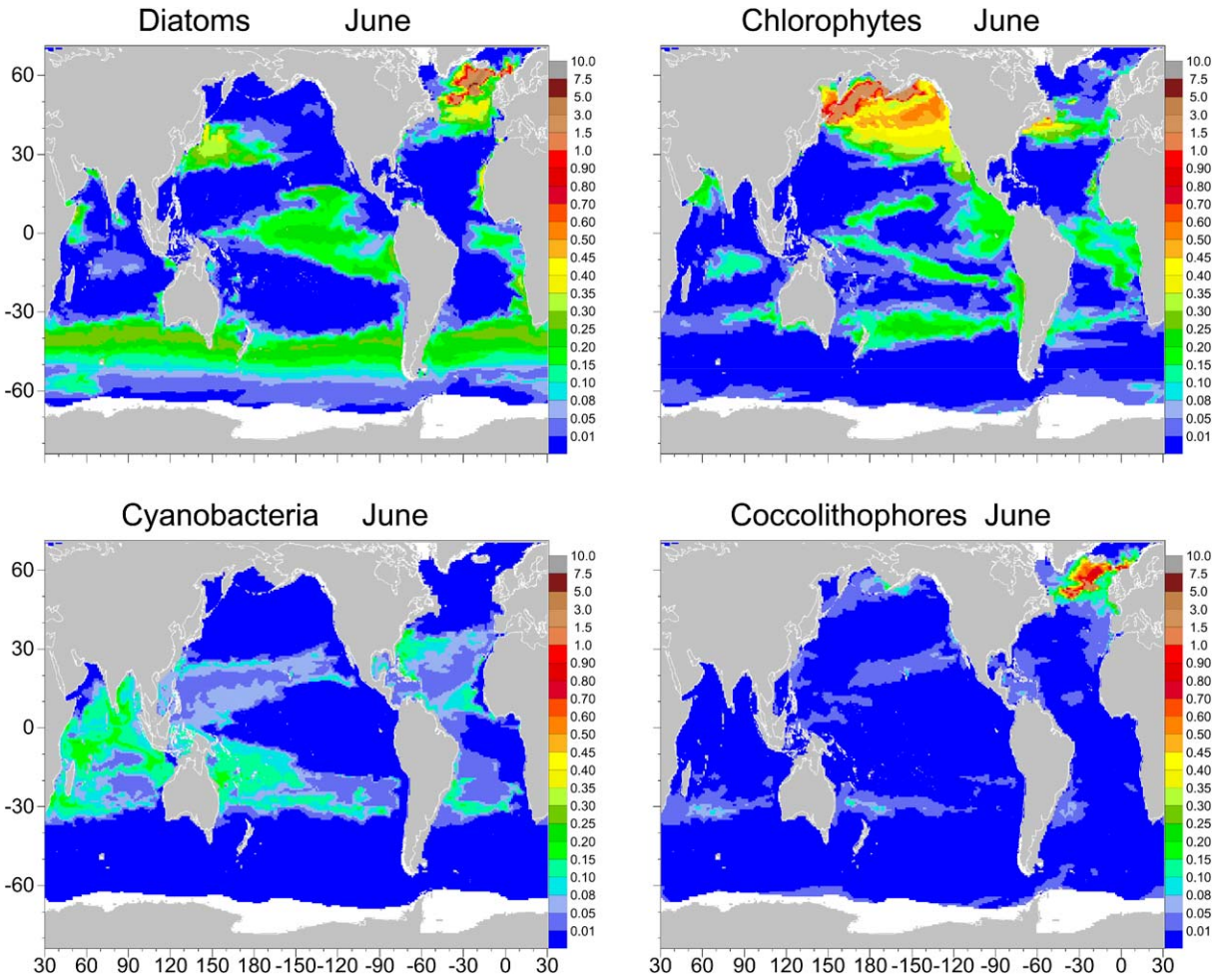

Fig. 9. Phytoplankton functional group distributions (as chlorophyll, mg m^{-3}) computed for June after 26 years of simulation. The groups were initialized as homogenous fields in the horizontal and vertical, at 0.05 mg m^{-3} everywhere. The distributions shown here represent values for a single day near the beginning of the month and not monthly means.

coccolithophore abundances overlap in the North Atlantic, while diatoms predominate the Antarctic Ocean and southern sub-polar transition region. Eynaud et al. (1999) found that diatoms were predominant in the Antarctic Ocean but also found that coccolithophores were abundant in the Antarctic sub-polar transition region, especially in the Atlantic sector where the observations were taken. Chlorophytes are found in high abundance the North Pacific and the edges of the equatorial upwelling regions outside the area dominated by diatoms. Chlorophytes/flagellates have been observed to be predominant in the eastern North Pacific (Thibault et al., 1999), where severe iron limitation limits diatom abundances, but diatoms have been observed in much higher concentrations elsewhere in the basin (Obayashi et al., 2001). Chlorophytes/flagellates have been characterized as occupying transitional regions (Ondrusek et al., 1991). Cyanobacteria are generally distributed throughout the central gyres at low concentrations, but have some larger abundances in the Indian basins, western central North Atlantic, and South Pacific (Fig. 9). The predominance of cyanobacteria in the mid-ocean gyres is well established (Glover, 1985; Itturiaga and Mitchell, 1986; Itturiaga and Marra, 1988).

In the model, diatoms follow the nutrients. Where there are abundant nutrient concentrations, diatoms tend to be prevalent. These regions occur in the model where kinetic energy is large: where convective overturn results in massive vertical displacement of water masses; where turbulent mixing processes are large; or where upwelling circulation is vigorous. These are the high latitudes, coastal upwelling areas, equatorial upwelling areas, and regions of strong monsoonal influences such as the Arabian Sea. This is because diatoms are the fastest growing of the functional groups in the model. This enables them to outcompete the other groups when nutrients and light are available. However, their large sinking rates prevent them from sustaining their populations in quiescent regions or periods.

Cyanobacteria are nearly the functional opposite of diatoms in the model. As slow growers, they cannot compete with diatoms under favorable growth conditions. But they have a competitive advantage in low nitrogen areas, by virtue of their uptake efficiency, low sinking rates, and to a minor extent their ability to fix molecular nitrogen. Thus they are abundant in quiescent regions, such as mid-ocean gyres, where circulation is sluggish, mixed layers are deep, and nutrients are only occasionally injected into the mixed layer. While they are able to survive in these regions, the lack of nutrients prevents them from attaining large concentrations.

Chlorophytes generally represent a transitional group in the model, inhabiting areas where nutrient and light availability are insufficient to allow diatoms to predominate, but not in areas where nutrients are so low as to prevent losses by sinking to compensate growth. This is a function of their intermediate growth, sinking, and nutrient uptake efficiency relative to diatoms and cyanobacteria. Their largest concentrations tend to be at the transition between the diatoms and cyanobacteria, such as the southern edge of the northern spring bloom (northern edge for the southern bloom), or the edges of the tropical upwelling and Arabian Sea blooms.

This concept of a transitional region between diatom-dominated upwelling and high-latitude regions, and cyanobacteria-dominated oligotrophic regions supports the suggestion by Ondrusek et al. (1991) for the greater North Pacific. In that study, this transitional region was occupied by a diverse assemblage of phytoplankton groups, as indicated by pigment analysis, and corresponding to the diverse definition of nanoflagellates in this analysis.

Similar overall distributions of the phytoplankton groups are observed in February as in June, except some facets are reversed in hemisphere (Fig. 10). Abundances of diatoms and coccolithophores have retreated southward in the North Atlantic. The austral spring bloom begins in the southern ocean and is predominantly diatoms, with chlorophytes at the periphery and coccolithophores in the southern portion. Cyanobacteria are again widely distributed and in low abundances, but with some patchy local blooms of modest magnitude.

High diatom abundances in the Equatorial Pacific run counter to observations in the region

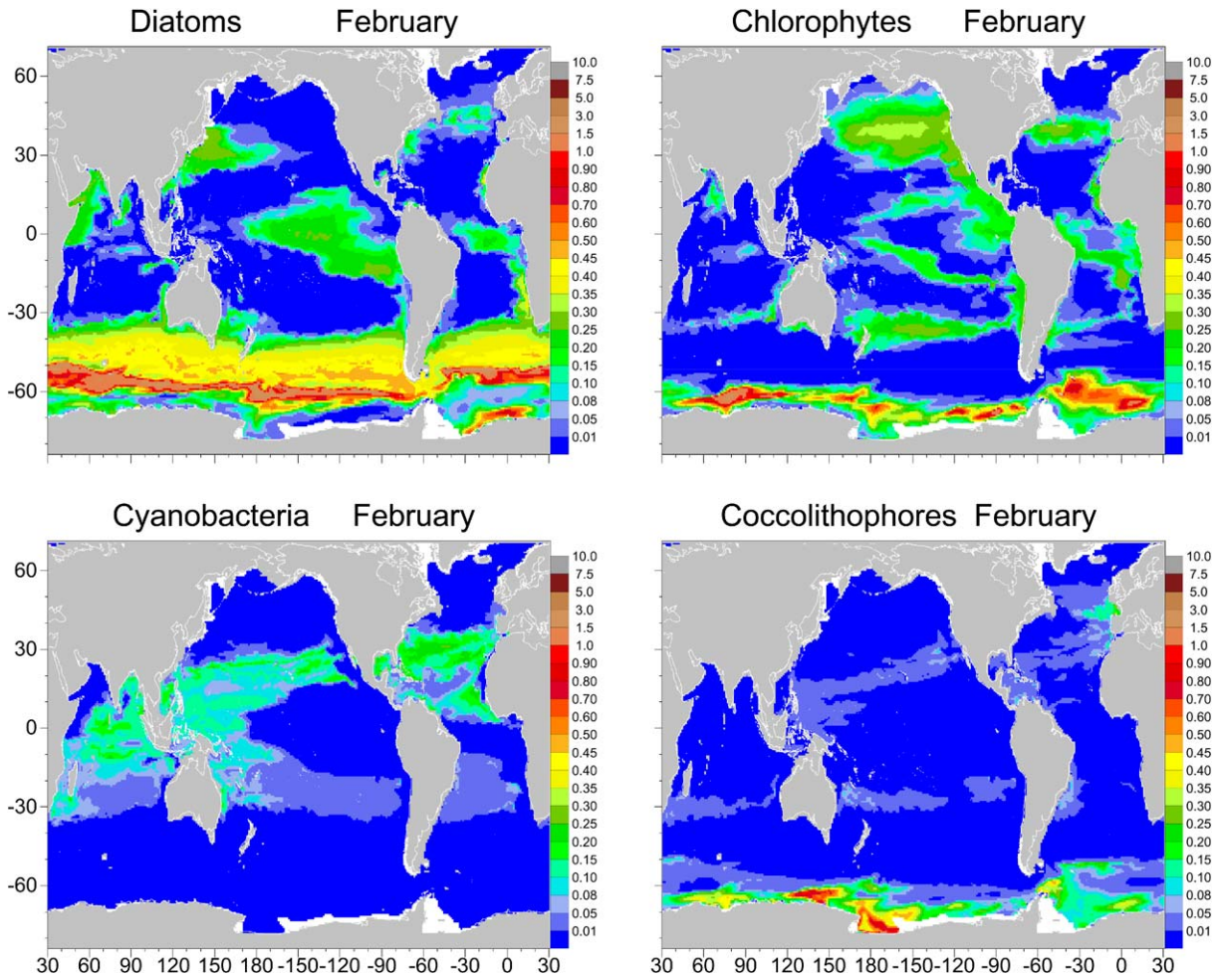

Fig. 10. Phytoplankton functional group distributions computed for February after 26 years of simulation. These represent values for a single day near the beginning of the month and not monthly means.

(e.g., Chavez, 1989; Landry et al., 1997; Brown et al., 1999), which indicate a pico–nano-plankton dominated community. This is most likely the result of excessive upwelling of dissolved iron in the model, as noted earlier. However, diatom abundance has been found to be larger very near the axis of the Pacific upwelling region (Landry et al., 1997), where iron availability is higher than outside of this band.

Seasonal variability of the phytoplankton groups is shown for four regions that are representative of most of the range of the global oceans (Fig. 11). The four regions are the North Atlantic (sub-polar region $>40°$N with pronounced spring bloom regions and fall/winter die-off), North Central Pacific (a low chlorophyll biomass central gyre, 10–40°N), North Indian Ocean (monsoon-dominated region, $>10°$N), and the Equatorial Atlantic (representing a tropical upwelling region, 10°S–10°N).

The North Atlantic exhibits a classic pattern of seasonal succession. Diatoms predominate early in the year as the mixed layer begins to shallow and light becomes readily available. They give way to dominance by coccolithophores in mid summer as the mixed layer stabilizes at shallow depth and

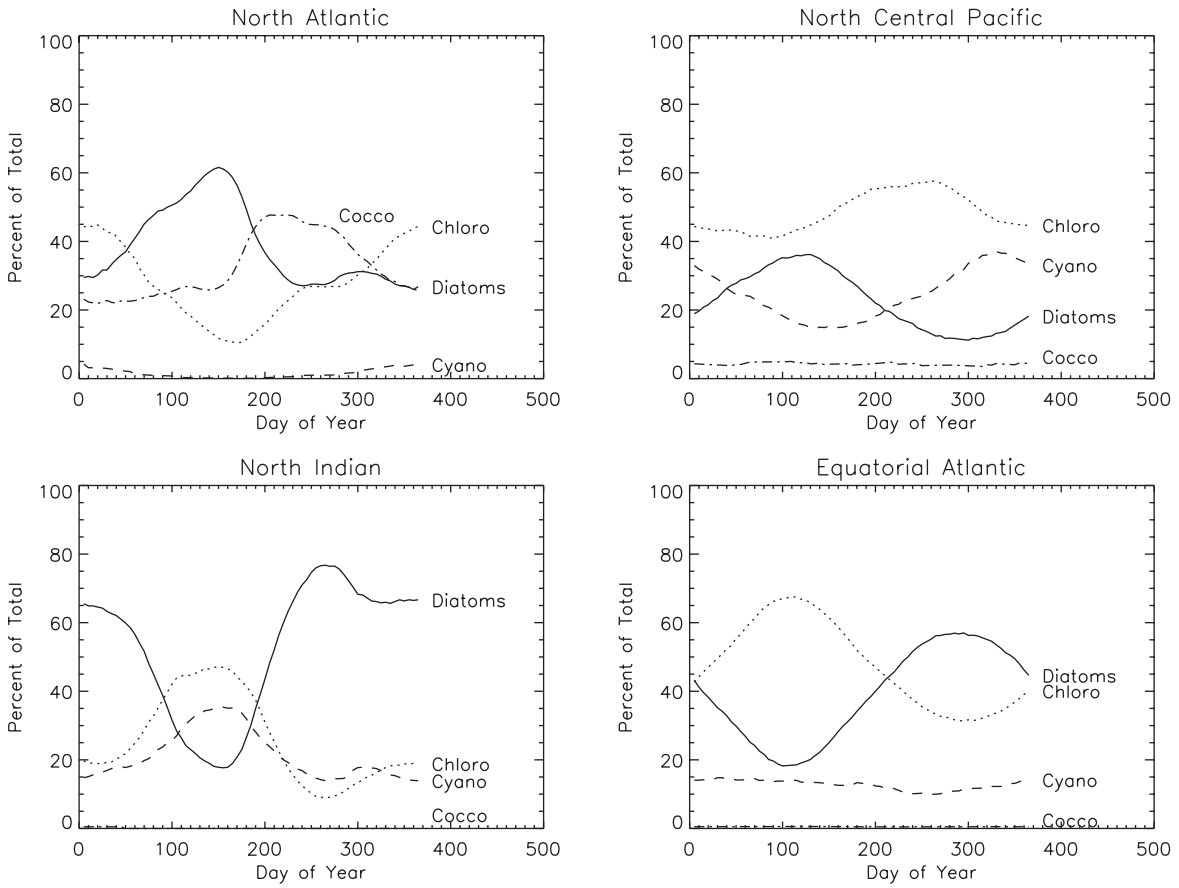

Fig. 11. Seasonal variability of phytoplankton groups in 4 regions, chosen to be representative of the range of most conditions in the global oceans. The groups are shown as proportion of the total in percent.

nutrients become limiting (Fig. 11). Chlorophytes reach a minimum at the diatom/coccolithophore dominance crossover, and increase late in the season matching and eventually exceeding coccolithophore relative abundances. Cyanobacteria provide a low and steady proportion of the total population, but increase slightly in the dead of boreal winter. This is due to their reduced losses from sinking relative to the others. Their concentrations diminish again when conditions for growth of diatoms improve.

Marañon et al. (2000) observed diatom predominance in the North Atlantic in May, up to 80% of the total phytoplankton carbon. They reported vastly reduced diatom relative abundances in Sep–Oct. Although Marañon et al. (2000) observed a significant proportion of cyanobacteria in both spring and autumn in the North Atlantic (about 25% of the total phytoplankton carbon), Gibb et al. (2001) found that they contributed a minor proportion of total chlorophyll, typically $<5\%$, as in the model.

The North Central Pacific exhibits a modest diatom spring bloom that never reaches community dominance (Fig. 11). Most of the year chlorophytes predominate, reaching highest levels of abundance in late summer into the autumn. They are located at the periphery of the equatorial upwelling and along the western US coast (Figs. 9 and 10). Late in the season, as nutrients reach their maximum level of depletion, cyanobacteria relative abundances rise. Coccolithophore relative

abundances do not exhibit substantial seasonal variability.

The North Indian Ocean is subject to four major seasonal influences, the southwest monsoon peaking in August, the less vigorous northeast monsoon occurring through the boreal winter, and two inter-monsoon periods between them. The abundances of diatoms follow the pattern of the monsoons, while cyanobacteria and chlorophytes respond more favorably to the inter-monsoon seasons (Fig. 11). This generally conforms to observations in the region (Brown et al., 1999). Stuart et al. (1998) showed that fucoxanthin, a biomarker for diatoms, increased 3- to 4-fold in the southwest monsoon from the inter-monsoon, concurrent with a nearly similar decrease in zeaxanthin, which is typically used to identify cyanobacteria. In the model, this is due to the presence of nutrients resulting from turbulence and upwelling associated with the monsoon periods, and favoring diatom growth. The extent of the diatom dominance is directly related to the strength of the monsoon period: they comprise nearly 80% in the more vigorous southwest monsoon compared to about 65% in the less vigorous northeast monsoon. Losses of diatoms from sinking in the inter-monsoon periods allow cyanobacteria and chlorophytes to outcompete the diatoms for the low concentrations of nutrients.

The Equatorial Atlantic exhibits a very different seasonal pattern from the other regions. In this region, chlorophytes dominate the total chlorophyll about half the year, yielding to diatoms in mid-to-late summer. These patterns follow the periods of upwelling in the Atlantic (Monger et al., 1997), which produce enough nutrient availability to allow diatom growth. Cyanobacteria and coccolithophores exhibit low relative abundances.

3.4. Comparisons of phytoplankton group distributions with in situ data

Comparison of model simulated phytoplankton distributions with in situ observations is mixed (Table 1). Generally, the observations show that diatoms are prevalent (> 15%) only in the North Atlantic, North Pacific, and Antarctic in the specific locations sampled. The model agrees with this, except that the North Pacific exhibits low diatom relative abundances due to iron limitation, and has large diatom abundances in the North Indian and Equatorial Pacific. Cyanobacteria are relatively abundant (> 10%) in the observations in the North Central Atlantic, North Central Pacific, North Indian, Equatorial Atlantic, Equatorial Pacific, South Atlantic, and South Pacific. The model patterns agree with the observed, except in the North Indian, where diatoms predominate in contrast to the observed cyanobacteria-predominance. The model typically under-represents the contribution of chlorophytes/flagellates, except in the North and Equatorial Pacific, where abundances are largely matched by the observations. The correspondence of model-derived coccolithophores with observations is generally very good, with model underestimates occurring in the central North Atlantic and Equatorial Pacific. Overall, chlorophyte/flagellate, cyanobacteria, and coccolithophore basin annual means were positively correlated with observations ($P<0.05$). Diatom annual means were not, deriving from discrepancies in the North Pacific (underestimated in the model) and North Indian (overestimated in the model) basins.

Regarding the community structure at the observation sites, some oceanographic basins exhibit a very strong correspondence with the in situ data. These include the North Central Pacific, Equatorial Atlantic, and South Atlantic. Other basins indicate agreement between some functional groups, but also areas of disagreement. Typically these disagreements occur in pairs, such as the Antarctic, where observations suggest a chlorophyte/flagellate-dominated community with diatoms secondary at the sites measured, while the model indicates the opposite at these same locations. Phytoplankton group relative abundances are not independent, and so a disagreement with one functional group will necessarily produce a disagreement with another. In the case of the Antarctic, the other phytoplankton groups indicate strong correspondence (Table 1). This is typical in this class of basins. Other basins in this category include the North Atlantic, North Pacific, North Central Atlantic, Equatorial Pacific, and the North Indian.

Table 1
Comparison of phytoplankton functional group distributions with observations

Basin		Data	Model	*N*
North Atlantic[1–6]	Diatoms	23%	54%	34
	Chlorophytes	40%	6%	23
	Cyanobacteria	8%	<1%	34
	Coccolithophores	36%	29%	11
North Pacific[7–9]	Diatoms	29%	<1%	58
	Chlorophytes	76%	97%	1
	Cyanobacteria	4%	<1%	58
	Coccolithophores	0%	1%	1
North Central Atlantic[2,6,10–14]	Diatoms	4%	15%	35
	Chlorophytes	19%	4%	16
	Cyanobacteria	43%	76%	45
	Coccolithophores	18%	2%	29
North Central Pacific[11,15,16]	Diatoms	4%	<1%	2
	Chlorophytes	20%	2%	1
	Cyanobacteria	62%	63%	23
	Coccolithophores	23%	27%	2
North Indian[17,18]	Diatoms	10%	83%	24
	Chlorophytes	27%	17%	12
	Cyanobacteria	44%	<1%	12
	Coccolithophores	5%	<1%	24
Equatorial Atlantic[6,10]	Diatoms	4%	16%	16
	Chlorophytes	N/A	—	0
	Cyanobacteria	59%	51%	16
	Coccolithophores	N/A	—	0
Equatorial Pacific[19–23]	Diatoms	11%	61%	23
	Chlorophytes	25%	20%	25
	Cyanobacteria	41%	17%	22
	Coccolithophores	19%	2%	23
South Atlantic[6]	Diatoms	2%	16%	24
	Chlorophytes	N/A	—	0
	Cyanobacteria	42%	47%	24
	Coccolithophores	N/A	—	0
South Pacific[21]	Diatoms	12%	21%	7
	Chlorophytes	32%	14%	7
	Cyanobacteria	42%	84%	2
	Coccolithophores	18%	5%	7
Antarctic[6,21,24–28]	Diatoms	28%	59%	73
	Chlorophytes	54%	14%	12
	Cyanobacteria	4%	<1%	59
	Coccolithophores	11%	5%	15

Table 1 (*continued*)

Basin		Data	Model	*N*
	Diatoms	Chlorophytes	Cyanobacteria	Coccolithophores
Correlation coefficients	0.26	0.82*	0.68*	0.80*

Results are expressed in percent of total phytoplankton population. For the model the total population is expressed as units of chlorophyll. For the observations, some are units of chlorophyll and some are units of carbon. *N* indicates the number of observations. N/A indicates no observations available for this basin. Percent abundances do not add up to 100% because not all groups were sampled in each observation, and because of averaging monthly and regionally. Correlation coefficients for the entire comparison are shown at the bottom. An asterisk indicates the correlation is significant at $P<0.05$. References are listed below. References: 1. Barlow et al. (1993); 2. Gibb et al. (2001); 3. Harris et al. (1997); 4. Holligan et al. (1993); 5. Malin et al. (1993); 6. Marañon et al. (2000); 7. Miller et al. (1991b); 8. Obayashi et al. (2001); 9. Thibault et al. (1999); 10. Agusti et al. (2001); 11. Andersen et al. (1996); 12. Claustre and Marty (1995); 13. DuRand et al. (2001); 14. Steinberg et al. (2001); 15. Campbell et al. (1997); 16. Letelier et al. (1993); 17. Barlow et al. (1999); 18. Tarran et al. (1999); 19. Blanchot et al. (2001); 20. Everitt et al. (1990) 21. Hardy et al. (1996); 22. Higgins and Mackey (2000); 23. Ishizaka et al. (1997); 24. Bathmann et al. (1997); 25. Brown and Landry (2001); 26. Gall et al. (2001) 27. Garrison et al. (1993); 28. Landry et al. (2001) 29. Peeken (1997); 30. van Leeuwe et al. (1998); 31. Wright et al. (1996).

The North Indian Ocean represents one of the largest disparities between the model and observations. The observations, located entirely in the Arabian Sea, indicate a modestly cyanobacteria-dominated community, whereas the model indicates a strongly diatom-dominated assemblage. Chlorophytes and coccolithophores are in reasonable agreement. The observations in the Arabian Sea are obtained from two sources, Tarran et al. (1999) and Barlow et al. (1999). Tarran et al. (1999) used cell counting methods and conversion to carbon based on biovolume and taxon-specific relationships in the literature, and showed massive cyanobacteria dominance even in the Southwest Monsoon. They found relatively low abundances of diatoms during the monsoon. If true, this represents the only bloom-magnitude (>1 mg m^{-3} chlorophyll) basin predominated by cyanobacteria in the global oceans that we are aware of. This also runs counter to the paradigm that low to moderate chlorophyll concentrations represent a "background" community composed of smaller phytoplankton, and blooms derive from an "excess" of diatoms above the background (Obayashi et al., 2001). With their low growth rates, low sinking rates, and high efficiency for uptaking nutrients, cyanobacteria are typically considered ideally suited for open-ocean gyres. Presence of nutrients in a strong upwelling environment, such as occurs in the SW monsoon, typically favors faster-growing phytoplankton, such as diatoms. This is what causes the predominance of diatoms in the model. Barlow et al. (1999), used pigment analysis at the same stations and times and found massive occurrences of fucoxanthin in the central Arabian Sea, up to 16 times more than the next most abundant pigment, in this case, 19′-hexanoyloxyfucoxanthin, a pigment commonly found in Prymnesiophytes (most likely coccolithophores here). It is unclear how to resolve these conflicting observations.

Both Tarran et al. (1999) and Barlow et al. (1999) found that during the autumn intermonsoon/early NE monsoon period, cyanobacteria became more abundant at the expense of diatoms. In the model, residual nitrate from the SW monsoon plus additional contributions from entrainment in the weaker NE monsoon provide sufficient nutrients for continued diatom predominance, although less so. However, in the spring intermonsoon, which is typically weaker then the autumn event, a changeover to increased cyanobacteria abundance did in fact occur in the model (Fig. 11), as would be expected from the observations.

Identification of phytoplankton functional group abundances and distributions is an emerging field in ocean biology. Detection of pigment composition using HPLC coupled with published algorithms for sorting the pigments into

phytoplankton taxonomic assemblages has given rise to a proliferation of reports in various oceanic locations. These new methodological advances are required because cell counting methods until very recently often did not include small phytoplankton, particularly cyanobacteria, and consequently the contributions of the larger phytoplankton, such as diatoms, were overestimated. Nevertheless, there is controversy in the application of the pigment approaches, with different algorithms being utilized to obtain functional group abundances. Thus comparisons between model output and observations must be viewed with caution in the light of these emerging methodologies, in addition to familiar model-data mismatches occurring because of interannual variability, spatial resolution discrepancies, extreme variability from investigator-to-investigator and sample-to-sample, among others. The comparison presented here is intended to be a first effort, and is not intended to be conclusive. There are clearly areas for encouragement in the simulation of multiple phytoplankton functional groups, but there remain many issues, both model-oriented and data-oriented, that remain to be resolved.

Acknowledgements

We wish to thank the JGOFS program for data collection and publication of special volumes that were essential to undertake a model validation effort. We thank Michele Rienecker, NASA/GSFC, Laboratory for Hydrospheric Processes, for critical comments on the manuscript. This work was supported under NASA Grant (RTOP) 971-291-08-04 and 971-622-51-31.

Appendix A. Model modifications description

The three-dimensional, coupled circulation/biogeochemical/radiative is based on Gregg (2000, 2002a). Modifications include iron limitation, introduction of a fourth phytoplankton functional group, and addition of a diatom detrital component. The governing equations of the iron-limiting model are

$$\frac{\partial}{\partial t}C_i = \nabla(K\nabla C_i) - \nabla\cdot\mathbf{V}C_i - \nabla\cdot(\mathbf{w}_s)_i C_i + \mu_i C_i - gC_iH - sC_i, \quad (A.1)$$

$$\frac{\partial}{\partial t}N_k = \nabla(K\nabla N_k) - \nabla\cdot\mathbf{V}N_k - b_k[\Sigma_i\mu_i C_I]_k + [b_k\varepsilon_k g\Sigma_i C_i]H + b_k\varepsilon_k s\Sigma_i C_i + b_k\varepsilon_k[n_1H + n_2H^2] + b_k r_k\Sigma_n D_n + A_k/H, \quad (A.2)$$

$$\frac{\partial}{\partial t}H = \nabla(K\nabla H) - \nabla\cdot\mathbf{V}H + [\Sigma_k(1-\varepsilon_k)g\Sigma_i C_i]H - n_1H - n_2H^2, \quad (A.3)$$

$$\frac{\partial}{\partial t}D_n = -\nabla\cdot(\mathbf{w}_d)_n D_n - \Sigma_k r_k D_n + \Sigma_k(1-\varepsilon_k)s\Sigma_i C_i + \Sigma_k(1-\varepsilon_k)[n_1H + n_2H^2], \quad (A.4)$$

where the subscripts k and i denote the existence of discrete quantities of nutrients (N, as nitrate, ammonium, silica, and iron) and chlorophyll (C, as diatoms, chlorophytes, cyanobacteria, and coccolithophores), and bold denotes a vector quantity. H represents herbivores. D represents detritus, where the subscript n denotes discrete quantities of diatom detritus (includes all detritus deriving from diatoms), and other detritus (all detritus deriving from the other phytoplankton groups). Thus for diatom detritus ($n=1$), the sum of C_i is only over 1 group (diatoms), while for other detritus ($n=2$), C_i is summed over the remaining groups ($i=2,3,4$). There is no advection/diffusion for detritus, but these processes resume after remineralization. We have found this approximation provides satisfactory results when the detrital sinking rates are kept relatively low, and it allows a major speed up in computational time. Other symbols are defined in Table 2. The only differences here from Gregg (2000, 2002a) are in Eq. (A.2) where a term for atmospheric deposition (A) is included, and only applies for iron (nmol m^{-2}), and in the two detrital quantities where before there was only one.

An additional modification deriving from the inclusion of iron is in the growth formulation,

Table 2
Notation and parameters and variables for the coupled three-dimensional ocean biogeochemical model

Symbol	Parameter/variable	Value	Units
K	Diffusivity	Variable	$m^2\ s^{-1}$
∇	Gradient operator	None	None
$\mathbf{V}$	Vector velocity	Variable	$m\ s^{-1}$
$\mathbf{w}_s$	Vector sinking rate of phytoplankton	0.0035–1.4	$m\ d^{-1}$
$\mathbf{w}_d$	Vector sinking rate of detritus		
	Diatom detritus	10.00	$m\ d^{-1}$
	Other detritus	3.0	$m\ d^{-1}$
μ	Specific growth rate of phytopl.	0–2.8	d^{-1}
b	Nutrient/chlorophyll ratio		
	Nitrogen	0.3–1.0	$\mu M(\mu g\ l^{-1})^{-1}$
	Silica	0.3–1.0	$\mu M(\mu g\ l^{-1})^{-1}$
	Iron	0.01–0.04	$nM(\mu g\ l^{-1})^{-1}$
ε	Nutrient regneration		
	Nitrate	0.0	d^{-1}
	Ammonium	0.25	d^{-1}
	Silica	0.0	d^{-1}
	Iron	0.25	d^{-1}
r	Remineralization rate	0–0.008	d^{-1}
A	Atmospheric deposition		
	Nitrogen	0.0	$\mu mol\ m^{-2}\ d^{-1}$
	Silica	0.0	$\mu mol\ m^{-2}\ d^{-1}$
	Iron	0.03–967.0	$nmol\ m^{-2}\ d^{-1}$
$K_{N,S,Fe}$	Half-saturation constant		
	Nitrogen	0.5–1.0	μM
	Silica	0.2	μM
	Iron	0.08–0.12	nM
g	Grazing rate by herbivores	0–2.15	d^{-1}
s	Senescence	0.05	d^{-1}
n_1, n_2	Hetrotrophic loss rates	0.1, 0.5	d^{-1}

Values are provided for the parameters and ranges are provided for the variables. Phytoplankton functional group-dependent physical and physiological parameters are shown in Fig. 2. The governing equations for the model are shown in Appendix A. Phytoplankton sinking rate and remineralization rates are variables because they are viscosity- and temperature-dependent, respectively. Phytoplankton specific growth rate is variable because of functional group and temperature-dependence. Nutrient/chlorophyll ratios are variable because of photadaptation-dependence (resulting in changes to carbon:chlorophyll ratio; see Gregg, 2000). Half-saturation constants are variables because of functional group dependence. Grazing and remineralization rates are variable because of temperature-dependence. A full description of grazing and circulation can be found in Gregg (2000).

which is

$$\mu_i = \mu_{mi}/\mu_{m1}\ \min[\mu(E_t)_i, \mu(N)_i, \mu(Si)_i, \mu(Fe)_i] \times \mu(T)\beta_i, \quad (A.5)$$

where I indicates the phytoplankton functional group index (in order, diatoms, chlorophytes, cyanobacteria, and coccolithophores), μ is the total specific growth rate (d^{-1}) of phytoplankton, μ_m is the maximum growth rate at 20°C (Fig. 2). The term $\mu(E_t)$ represents the growth rate, as a function solely of the total irradiance ($\mu mol\ quanta\ m^{-2}\ s^{-1}$),

$$\mu(E_t) = \frac{E_t}{(E_t + k_E)}, \quad (A.6)$$

where k_E is the irradiance at which $\mu = 0.5\mu_m$ and equals 0.5 I_k, where I_k is the light saturation parameter. $\mu(N)$ is the growth rate determined by total nitrogen concentration including nitrate (NO_3) and ammonium (NH_4), $\mu(Si)$ is the growth rate as a function of silica concentration, $\mu(Fe)$ is the growth rate as a function of iron concentration, and $\mu(T)$ is the temperature-dependence of

Table 3
Tabulated values of phytoplankton group parameters

	Diatoms	Chlorophytes	Cyanobacteria	Coccolithophores
Maximum growth rate at 30°C (d^{-1})	2.0	1.73	1.34	1.51
Sinking rate (m d^{-1})	1.5	0.25	0.00085	0.3–1.4
Light saturation (μmol quanta m^{-2} s^{-1})				
Low light (50)	90.0	96.9	65.1	56.1
Medium light (150)	93.0	87.0	66.0	71.2
High light (200)	184.0	143.7	47.1	165.4
Half-saturation nitrogen (μM)	1.0	0.75	0.5	0.5
Half-saturation iron (nM)	0.12	0.10	0.10	0.08

growth (Eppley, 1972)

$$\mu(\mathrm{NO_3})_i = \frac{\mathrm{NO_3}}{[\mathrm{NO_3} + (k_\mathrm{N})_i]}, \tag{A.7}$$

$$\mu(\mathrm{NH_4})_i = \frac{\mathrm{NH_4}}{[\mathrm{NH_4} + (k_\mathrm{N})_i]}, \tag{A.8}$$

$$\mu(\mathrm{N})_i = \mu(\mathrm{NH_4})_i + \min[\mu(\mathrm{NO_3})_i, 1 - \mu(\mathrm{NH_4})_i] \tag{A.9}$$

(Gregg and Walsh, 1992)

$$\mu(\mathrm{Si})_i = \frac{\mathrm{Si}}{[\mathrm{Si} + (k_\mathrm{S})_i]}, \tag{A.10}$$

$$\mu(\mathrm{Fe})_i = \frac{\mathrm{Fe}}{[\mathrm{Fe} + (k_\mathrm{F})_i]}, \tag{A.11}$$

$$\mu(T) = (0.851\alpha\, 1.066^T), \tag{A.12}$$

where α is a factor to convert to units of d^{-1} (instead of doublings d^{-1}) and to adjust for a 12-h photoperiod ($\alpha = 0.347$), and β is an additional adjustment used for the cyanobacteria component that reduces their growth rate in cold water (<15°C)

$$\beta_3 = 0.0294T + 0.558 \tag{A.13}$$

(Gregg, 2000). $\beta_i = 1$ for the other three phytoplankton components ($i = 1, 2, 4$). This effect conforms to observations that cyanobacteria are scarce in cold waters (Agawin et al., 1998, 2000; Li, 1998). The cyanobacteria component possesses a modest ability to fix nitrogen from the water column, as observed in *Trichodesmium* spp. (Carpenter and Romans, 1991). The nitrogen fixation is expressed as 0.001 the light-limited growth rate, and only applies when nitrate availability is $<(k_\mathrm{N})_3$, where the index 3 indicates cyanobacteria. The fixed nitrogen is dentrified by the detrital component to prevent nitrogen accumulation in the model domain.

Photoadaptation is simulated by postulating three states: 50, 150 and 200 (μmol quanta m^{-2} s^{-1}). This is based on laboratory studies which typically divide experiments into low, medium, and high classes of light adaptation. Carbon:chlorophyll (C:chl) ratios are related directly to the photoadaptation state. This simulates the behavior of phytoplankton to preferentially synthesize chlorophyll in low light conditions, to enable more efficient photon capture. These three C:chl states are 25, 50 and 80 g g^{-1} (Table 3). The C:chl classification is important for determining the nutrient:chlorophyll ratios, which are computed assuming the Redfield elemental balances (6.625 C:N and C:Si ratios) and 150 C:Fe ratio (μmol:nmol)

$$b_\mathrm{N,Si} = (\mathrm{C:chl})/79.5, \tag{A.14}$$

$$b_\mathrm{F} = (\mathrm{C:chl})/1800.0. \tag{A.15}$$

There are several recent advances in modeling phytoplankton photoadaptation (e.g., Anning et al., 2000; Han et al., 1999; Geider et al., 1998; Zonneveld, 1997). However, a comprehensive description of multiple phytoplankton groups remains lacking. Our simulation of photoadaptation was gleaned from carefully controlled, intercomparative laboratory experiments available in the general literature (Perry et al., 1981; Wyman and Fay, 1986; Langdon, 1987; Sakshaug and Andresen, 1986; Bates and Platt, 1984; Barlow and Alberte, 1985). Care was taken to utilize studies

for which temperature, growth irradiance, and light:dark cycles were very similar so that phytoplankton functional group comparisons were valid. The low light and high light-adapted values correspond to recent modeling efforts. For example, using Anning et al.'s (2000) formulation for chlorophyll:carbon ratios and Geider et al.'s (1998) data for *Skeletonema costatum*, we derive low light-adapted C:chl of 35 g g^{-1}, which compares favorably to our specified value of 25 g g^{-1}. Similarly the high light-adapted value is 73 g g^{-1}, compared to our value of 80 g g^{-1}. An intermediate value derived by taking the mean is 55 g g^{-1}, which compares favorably to our value of 50 g g^{-1}.

We compute the mean irradiance during daylight hours, and then classify the phytoplankton photoadaptive state accordingly. This calculation is only performed once per day to simulate a delayed photoadaptation response.

References

Agawin, N.S.R., Duarte, C.M., Agusti, S., 1998. Growth and abundance of *Synechococcus* sp. in a Mediterranean Bay: seasonality and relationship with temperature. Marine Ecology Progress Series 170, 45–53.

Agawin, N.S.R., Duarte, C.M., Agusti, S., 2000. Nutrient and temperature control of the contribution of picoplankton to phytoplankton biomass and production. Limnology and Oceanography 45, 591–600.

Agusti, S., Duarte, C.M., Vaque, D., Hein, M., Gasol, J.M., Vidal, M., 2001. Food-web structure and elemental (C, N and P) fluxes in the eastern tropical North Atlantic. Deep-Sea Research II 48, 2295–2321.

Andersen, R.A., Bidigare, R.R., Keller, M.D., Latasa, M., 1996. A comparison of HPLC pigment signatures and electron microscopic observations for oligotrophic waters of the North Atlantic and Pacific Oceans. Deep-Sea Research II 43, 517–537.

Anning, T., Maclntyre, H.L., Pratt, S.M., Sammes, P.J., Gibb, S., Geider, R.J., 2000. Photoacclimation in the marine diatom *Skeletonema costatum*. Limnology and Oceanography 45, 1807–1817.

Archer, D.E., Johnson, K., 2000. A model of the iron cycle in the ocean. Global Biogeochemical Cycles 14, 269–279.

Barlow, R.G., Alberte, R.S., 1985. Photosynthetic characteristics of phycoerythrin-containing marine *Synechococcus* spp. Marine Biology 86, 63–74.

Barlow, R.G., Mantoura, R.F.C., Gough, M.A., Fileman, T.W., 1993. Pigment signatures of the phytoplankton composition in the northeastern Atlantic during the 1990 spring bloom. Deep-Sea Research II 40, 459–477.

Barlow, R.G., Mantoura, R.F.C., Cummings, D., 1999. Monsoonal influences in the distribution of phytoplankton pigments in the Arabian Sea. Deep-Sea Research II 46, 677–699.

Bates, S.S., Platt, T., 1984. Fluorescence induction as a measure of photosynthetic capacity in marine phytoplankton: response of *Thalassiosira pseudonana* (Bacillariophyceae) and *Dunaliella tertiolecta* (Chlorophyceae). Marine Ecology Progress Series 18, 67–77.

Bathmann, U.V., Scharek, R., Klaas, C., Dubischar, C.D., Smetacek, V., 1997. Spring development of phytoplankton biomass and composition in major water masses of the Atlantic sector of the Southern Ocean. Deep-Sea Research II 44, 51–67.

Bidigare, R.R., Morrow, J.H., Kiefer, D.A., 1989. Derivative analysis of spectral absorption by photosynthetic pigments in the western Sargasso Sea. Journal of Marine Research 47, 323–341.

Blanchot, J., Andre, J.-M., Navarette, C., Neveux, J., Radenac, M.-H., 2001. Picophytoplankton in the equatorial Pacific: Vertical distributions in the warm pool and in the high nutrient low chlorophyll conditions. Deep-Sea Research I 48, 297–314.

Bowie, A.R., Whitworth, D.J., Achterberg, E.P., Fauzi, R., Mantoura, C., Worsfold, P.J., 2002. Biogeochemistry of Fe and other trace elements (Al, Co, Ni) in the upper Atlantic Ocean. Deep-Sea Research I 49, 605–636.

Boyd, P., Pomroy, A., Bury, S., Savidge, G., Joint, I., 1997. Micro-algal carbon and nitrogen uptake in post-coccolithophore bloom conditions in the northeast Atlantic, July, 1991. Deep-Sea Research I 44, 1497–1517.

Boyd, P.W. and 34 others, 2000. A mesoscale phytoplankton bloom in the polar Southern Ocean stimulated by iron fertilization. Nature 407, 695–702.

Brand, L.E., 1991. Minimum iron requirements of marine phytoplankton and the implications for the biogeochemical control of new production. Limnology and Oceanography 36, 1756–1771.

Brand, L.E., Sunda, W.G., Guillard, R.R.I., 1983. Limitation of marine phytoplankton reproductive rates by zinc, manganese, and iron. Limnology and Oceanography 28, 1182–1198.

Brand, L.E., Sunda, W.G., Guillard, R.R.L., 1986. Reduction of marine phytoplankton reproduction rates by copper and cadmium. Journal of Experimental Marine Biology and Ecology 96, 225–250.

Brown, C.W., Yoder, J.A., 1994. Coccolithophorid blooms in the global ocean. Journal of Geophysical Research 99, 7467–7482.

Brown, S.L., Landry, M.R., 2001. Mesoscale variability in biological community structure and biomass in the Antarctic polar front region at 170°W during austral spring 1997. Journal of Geophysical Research 106, 13917–13930.

Brown, S.L., Landry, M.R., Barber, R.T., Campbell, L., Garrison, D.L., Gowing, M.M., 1999. Picophytoplankton

dynamics and production in the Arabian Sea during the 1995 southwest monsoon. Deep-Sea Research II 46, 1745–1768.

Bucciarelli, E., Blain, S., Treguer, P., 2001. Iron and manganese in the wake of the Kerguelen Islands (Southern Ocean). Marine Chemistry 73, 21–36.

Campbell, L., Liu, H., Nolla, H.A., Vaulot, D., 1997. Annual variability of phytoplankton and bacteria in the subtropical North Pacific Ocean at Station ALOHA during the 1991–1994 ENSO event. Deep-Sea Research I 44, 167–192.

Carpenter, E.J., Romans, K., 1991. Major role of the cyanobacterium *Trichodesmium* in nutrient cycling in the North Atlantic Ocean. Science 254, 1356–1358.

Chavez, F.P., 1989. Size distribution of phytoplankton in the central and eastern tropical Pacific. Global Biogeochemical Cycles 3, 27–35.

Chavez, F.P., Strutton, P.G., Friederich, G.E., Feely, R.A., Feldman, G.C., Foley, D.G., McPhaden, M.J., 1999. Biological and chemical response of the Equatorial Pacific to the 1997–98 El Niño. Science 286, 2126–2131.

Christian, J.R., Verschell, M.A., Murtugudde, R., Busalacchi, A.J., McClain, C.R., 2002. Biogeochemical modeling of the tropical Pacific Ocean II: iron biogeochemistry. Deep-Sea Research II 49, 545–565.

Claustre, H., Marty, J.-C., 1995. Specific phytoplankton biomasses and their relation to primary production in the tropical North Atlantic. Deep-Sea Research I 42, 1475–1493.

Coale, K.H., Fitzwater, S.E., Gordon, R.M., Johnson, K.S., Barber, R.T., 1996. Control of community growth and export production by upwelled iron in the Equatorial Pacific Ocean. Nature 379, 621–624.

Coale, K.H., Johnson, K.S., Fitzwater, S.E., Blain, S.O.G., Stanton, T.P., Coley, T.L., 1998. Iron Ex-I, and in situ iron-enrichment experiment: experimental design, implementation, and results. Deep-Sea Research II 45, 919–945.

Conkright, M.E., Levitus, S., Boyer, T.P., 1994. World Ocean Atlas, Vol. 1: nutrients. NOAA Atlas NESDIS, Vol. 1, 150pp. US Govt Printing Office, Washington DC.

Conkright, M.E., O'Brien, T., Levitus, S., Boyer, T.P., Stephens, C., Antonov, J., 1998. World Ocean Atlas 1998, Vol. 12: nutrients and chlorophyll of the Indian Ocean. NOAA Atlas NESDIS, Vol. 38, 217pp. US Govt Printing Office, Washington DC.

de Baar, H.J.W., de Jong, J.T.M., Bakker, D.C.E., Loscher, B.M., Veth, C., Bathmann, U., Smetacek, V., 1995. Importance of iron for plankton blooms and carbon dioxide drawdown in the Southern Ocean. Nature 373, 412–415.

de Baar, H.J.W., de Jong, J.T.M., Nolting, R.F., Timmermans, K.R., van Leeuwe, M.A., Bathmann, U., van der Loeff, M.R., Sildam, J., 1999. Low dissolved Fe and the absence of diatom blooms in remote Pacific waters of the Southern Ocean. Marine Chemistry 66, 1–34.

DiTullio, G.R., Hutchins, D.A., Bruland, K.W., 1993. Interaction of iron and major nutrients controls phytoplankton growth and species composition in the tropical North Pacific Ocean. Limnology and Oceanography 38, 495–508.

DuRand, M.D., Olson, R.J., Chisholm, S.W., 2001. Phytoplankton population dynamics at the Bermuda Atlantic Time-series station in the Sargasso Sea. Deep-Sea Research II 48, 1983–2003.

Eppley, R.W., 1972. Temperature and phytoplankton growth in the sea. Fisheries Bulletin 70, 1063–1085.

Eppley, R.W., Rogers, J.N., McCarthy, J.J., 1969. Half-saturation constants for uptake of nitrate and ammonium by marine phytoplankton. Limnology and Oceanography 14, 912–920.

Everitt, D., Wright, S., Volkman, J.K., Thomas, D.P., Lindstrom, E.J., 1990. Phytoplankton community compositions in the western equatorial Pacific determined from chlorophyll and carotenoid pigment distributions. Deep-Sea Research 37, 975–997.

Eynaud, F., Girardeau, J., Pichon, J.-J., Pudsey, C.J., 1999. Sea-surface distribution of coccolithophores, diatoms, silicoflagellates, and dinoflagellates in the South Atlantic Ocean during the late austral summer 1995. Deep-Sea Research I 146, 451–482.

Falkowski, P.G., Dubinsky, G.Z., Wyman, K., 1985. Growth-irradiance relationships in phytoplankton. Limnology and Oceanography 30, 311–321.

Fitzwater, S.E., Coale, K.H., Gordon, R.M., Johnson, K.S., Ondrusek, M.E., 1996. Iron deficiency and phytoplankton growth in the equatorial Pacific. Deep-Sea Research II 43, 995–1015.

Fritz, J.J., Balch, W.M., 1996. A light-limited continuous culture study of *Emiliana huxleyi*: determination of coccolith detachment and its relevance to cell sinking. Journal of Experimental Marine Biology and Ecology 207, 127–147.

Fung, I.Y., Meyn, S.K., Tegen, I., Doney, S.C., John, J.G., Bishop, J.K.B., 2000. Iron supply and demand in the upper ocean. Global Biogeochemical Cycles 14, 281–295.

Gall, M.P., Boyd, P.W., Hall, J., Safi, K.A., Chang, H., 2001. Phytoplankton processes. Part 1: community structure during the Southern Ocean Iron Release Experiment (SOIREE). Deep-Sea Research II 48, 2551–2570.

Garrison, D.L., Buck, K., Gowing, M.M., 1993. Winter plankton assemblage in the ice edge zone of the Weddell and Scotia Seas: composition, biomass and spatial distribution. Deep-Sea Research I 40, 311–338.

Gavis, J., Guillard, R.R.L., Woodward, B.L., 1981. Cupric ion activity and the growth of phytoplankton clones isolated from different marine environments. Journal of Marine Research 39, 315–333.

Geider, R.J., Maclntyre, H.L., Kana, T.M., 1998. A dynamic regulatory model of phytoplanktonic acclimation to light, nutrients, and temperature. Limnology and Oceanography 43, 679–694.

Gibb, S.W., Cummings, D.G., Irigoien, X., Barlow, R.G., Fauzi, R., Mantoura, C., 2001. Phytoplankton pigment chemotaxonomy of the northeastern Atlantic. Deep-Sea Research II 48, 795–823.

Ginoux, P., Chin, M., Tegen, I., Prospero, J.M., Holben, B., Dubovik, O., Lin, S.-J., 2001. Sources and distributions of

dust aerosols simulated with the GOCART model. Journal of Geophysical Research 106, 20255–20273.

Gledhill, M., van den Berg, C.M.G., Nolting, R.F., Timmermans, K.R., 1998. Variability in the speciation of iron in the northern North Sea. Marine Chemistry 59, 283–300.

Glover, H.E., 1985. The physiology and ecology of the marine cyanobacterial genus *Synechococcus*. Advances in Microbiology 3, 49–107.

Gordon, R.M., Johnson, K.S., Coale, K.H., 1998. The behavior of iron and other trace elements during the IronEx I and PlumEx experiments in the equatorial Pacific. Deep-Sea Research II 45, 995–1041.

Gregg, W.W., 2000. A coupled ocean general circulation, biogeochemical, and radiative model of the global oceans: seasonal distributions of ocean chlorophyll and nutrients. NASA Technical Memorandum 2000-209965, 33pp. (Available online from anonymous ftp at salmo.gsfc.nasa.gov, directory location pub/outgoing/reprints/nasatm2000.pdf)

Gregg, W.W., 2002a. Tracking the SeaWiFS record with a coupled physical/biogeochemical/radiative model of the global oceans. Deep-Sea Research II 49, 81–105.

Gregg, W.W., 2002b. A coupled ocean-atmosphere radiative model for global ocean biogeochemical models. In: Suarez, M. (Ed.), NASA Global Modeling and Assimilation Series, NASA Technical Memorandum, 2002-104606, Vol. 22, 33pp. (Available online from anonymous ftp at salmo.gsfc.nasa.gov, directory location pub/outgoing/reprints/nasatm2002.pdf)

Gregg, W.W., Walsh, J.J., 1992. Simulation of the 1979 spring bloom in the Mid-Atlantic Bight: a coupled physical/biological/optical model. Journal of Geophysical Research 97, 5723–5743.

Hall, J.A., Safi, K., 2001. The impact of in situ Fe fertilisation on the microbial food web in the Southern Ocean. Deep-Sea Research II 48, 2591–2613.

Han, B.-P., Virtanen, M., Koponen, J., Straskraba, M., 1999. Predictors of light-limited growth and competition of phytoplankton in a well-mixed water column. Journal of Theoretical Biology 197, 439–450.

Hardy, J., Hanneman, A., Behrenfeld, M., Horner, R., 1996. Environmental biogeography of near-surface phytoplankton in the southeast Pacific Ocean. Deep-Sea Research I 43, 1647–1659.

Harris, R.P., Boyd, P., Harbour, D.S., Head, R.N., Pingree, R.D., Pomroy, A.J., 1997. Physical, chemical and biological features of a cyclonic eddy in the region of 61°10′N 10°50′W in the North Atlantic. Deep-Sea Research I 44, 1815–1839.

Higgins, H.W., Mackey, D.J., 2000. Algal class abundances, estimated from chlorophyll and carotenoid pigments, in the western Equatorial Pacific under El Niño and non-El Niño conditions. Deep-Sea Research I 47, 1461–1483.

Holligan, P.M., Fernandez, E., Aiken, J., Balch, W.M., Boyd, P., Burkill, P.H., Finch, M., Groom, S.B., Malin, G., Muller, K., Purdie, D.A., Robinson, C., Trees, C.C., Turner, S.M., van der Waal, P., 1993. A biogeochemical study of the coccolithophore, *Emiliana huxleyi*, in the North Atlantic. Global Biogeochemical Cycles 7, 879–900.

Iglesias-Rodriguez, M.D., Brown, C.W., Doney, S.C., Kleypas, J., Kolber, D., Kolber, Z., Hayes, P.K., Falkowski, P.G., 2002. Representing key phytoplankton functional groups in ocean carbon cycle models: coccolithophorids. Global Biogeochemical Cycles 16 (4), 1100 (doi: 10.1029/2001BG001454).

Ishizaka, J., Harada, K., Ishikawa, K., Kiyosawa, H., Furusawa, H., Watanabe, Y., Ishida, H., Suzuki, K., Handa, N., Takahashi, M., 1997. Size and taxonomic plankton community structure and carbon flow at the equator, 175°E during 1990–1994. Deep-Sea Research II 44, 1927–1949.

Itturiaga, R., Marra, J., 1988. Temporal and spatial variability of chroccoid cyanobacteria *Synechococcus* spp. specific growth rates and their contribution to primary productivity in the Sargasso Sea. Marine Ecology Progress Series 44, 175–181.

Itturiaga, R., Mitchell, B.G., 1986. Chrococcoid cyanobacteria: a significant component in the food web dynamics of the open ocean. Marine Ecology Progress Series 28, 291–297.

Johnson, K.S., Gordon, R.M., Coale, K.H., 1997. What controls dissolved iron concentrations in the world ocean? Marine Chemistry 57, 137–161.

Johnson, K.S., Chavez, F.P., Elrod, V.A., Fitzwater, S.E., Pennington, J.T., Buck, K.R., Walz, P.M., 2001. The annual cycle of iron and the biological response in central California coastal waters. Geophysical Research Letters 28, 1247–1250.

Kolber, Z.S., Barber, R.T., Coale, K.H., Fitzwater, S.E., Greene, R.M., Johnson, K.S., Lindley, S., Falkowski, P.G., 1994. Iron limitation of phytoplankton photosynthesis in the equatorial Pacific Ocean. Nature 371, 145–148.

Landry, M.R., Barber, R.T., Bidigare, R.R., et al., 1997. Iron and grazing constraints on primary/production in the central equatorial Pacific: an EqPac synthesis. Limnology and Oceanography 42, 405–418.

Landry, M.R., Brown, S.L., Selph, K.E., Abbott, M.R., Letelier, R.M., Christensen, S., Bidigare, R.R., Casciotti, K., 2001. Initiation of the spring phytoplankton increase in the Antarctic polar front zone at 170°W. Journal of Geophysical Research 106, 13903–13915.

Langdon, C., 1987. On the causes of interspecific differences in the growth–irradiance relationship for phytoplankton. Part I. A comparative study of the growth–irradiance relationship of three marine phytoplankton species: *Skeletonema costatum*, *Olisthodiscus luteus*, and *Gonyaulax tamarensis*. Journal of Plankton Research 9, 459–482.

Leonard, C.L., McClain, C.R., Murtugudde, R., Hofmann, E.E., Harding, L.W., 1999. An iron-based ecosystem model of the central equatorial Pacific. Journal of Geophysical Research 104, 1325–1341.

Letelier, R.M., Bidigare, R.R., Hebel, D.V., Ondrusek, M., Winn, C.D., Karl, D.M., 1993. Temporal variability of phytoplankton community structure based on pigment analysis. Limnology and Oceanography 38, 1420–1437.

Li, W.K.W., 1998. Annual average abundance of heterotrophic bacteria and *Synechococcus* in surface ocean waters. Limnology and Oceanography 43, 1746–1753.

Loscher, B.M., de Baar, H.J.W., de Jong, J.T.M., Veth, C., Dehairs, F., 1997. The distribution of Fe in the Antarctic circumpolar current. Deep-Sea Research II 44, 143–187.

Mackey, D.J., Blanchot, J., Higgins, W.W., Neveux, J., 2002. Phytoplankton abundances and community structure in the equatorial Pacific. Deep-Sea Research II 49, 2561–2582.

Malin, G., Turner, S., Liss, P., Holligan, P., Harbour, D., 1993. Dimethylsulphide and dimethylsulphoniopropionate in the Northeast Atlantic during the summer coccolithophore bloom. Deep-Sea Research I 40, 1487–1508.

Mann, E.L., Chisholm, S.W., 2000. Iron limits the cell division rate of *Prochlorococcus* in the eastern equatorial Pacific. Limnology and Oceanography 45, 1067–1076.

Marañon, E., Holligan, P.M., Varela, M., Mouriño, B., Bale, A.J., 2000. Basin-scale variability of phytoplankton biomass and growth in the Atlantic Ocean. Deep-Sea Research I 47, 825–857.

Martin, J.H., Gordon, R.M., 1988. Northeast Pacific iron distributions in relation to phytoplankton productivity. Deep-Sea Research 35, 177–196.

Martin, J.H., Gordon, R.M., Fitzwater, S., Broenkow, W.W., 1989. VERTEX: phytoplankton/iron studies in the Gulf of Alaska. Deep-Sea Research 36, 649–680.

Martin, J.H., Gordon, R.M., S.E. Fitzwater, S.E., 1990. Iron in Antarctic waters. Nature 345, 156–158.

Martin, J.H., Fitzwater, S.E., Gordon, R.M., Hunter, C.N., Tanner, S.J., 1993. Iron, primary production and carbon–nitrogen flux studies during the JGOFS North Atlantic spring bloom experiment. Deep-Sea Research II 40, 115–134.

Measures, C.I., Vink, S., 1999. Seasonal variations in the distribution of Fe and Al in the surface waters of the Arabian Sea. Deep-Sea Research II 46, 1597–1622.

Measures, C.I., Vink, S., 2001. Dissolved Fe in the upper waters of the Pacific sector of the Southern Ocean. Deep-Sea Research II 48, 3913–3941.

Miller, C.B., Frost, B.W., Wheeler, P.A., Landry, M.R., Welschmeyer, N., Powell, T.M., 1991a. Ecological dynamics in the subarctic Pacific, a possibly iron-limited system. Limnology and Oceanography 36, 1600–1615.

Miller, C.B., Frost, B.W., Booth, B., Wheeler, P.A., Landry, M.R., Welschmeyer, N., 1991b. Ecological processes in the subarctic Pacific: iron limitation cannot be the whole story. Oceanography 4, 71–78.

Monger, B., McClain, C., Murtugudde, R., 1997. Seasonal phytoplankton dynamics in the eastern tropical Atlantic. Journal of Geophysical Research 102, 12389–12411.

Moore, J.K., Doney, S.C., Glover, D.M., Fung, I.Y., 2002. Iron cycling and nutrient-limitation patterns in the surface waters of the world ocean. Deep-Sea Research II 49, 463–507.

Morel, F.M.M., Hudson, R.J.M., Price, N.M., 1991a. Limitation of productivity by trace metals in the sea. Limnology and Oceanography 36, 1742–1755.

Morel, F.M.M., Rueter, J.G., Price, N.M., 1991b. Iron nutrition of phytoplankton and its possible importance in the ecology of open ocean regions with high nutrient and low biomass. Oceanography 4, 56–61.

Moulin, C., Gordon, H.R., Chomko, R.M., Banzon, V.F., Evans, R.H., 2001. Atmospheric correction of ocean color imagery through thick layers of Saharan dust. Geophysical Research Letters 28, 5–8.

Nakabayashi, S., Kusakabe, M., Kuma, K., Kudo, I., 2001. Vertical distributions of Iron (III) hydroxide solubility and dissolved iron in the northwestern North Pacific Ocean. Geophysical Research Letters 28, 4611–4614.

Obayashi, Y., Tanoue, E., Suzuki, K., Handa, N., Nojiri, Y., Wong, C.S., 2001. Spatial and temporal variabilities of phytoplankton community structure in the northern north Pacific as determined by phytoplankton pigments. Deep-Sea Research I 48, 439–469.

Ondrusek, M.E., Bidigare, R.R., Sweet, S.T., Defreitas, D.A., Brooks, J.M., 1991. Distribution of phytoplankton pigments in the North Pacific Ocean in relation to physical and optical variability. Deep-Sea Research 38, 243–266.

Oschlies, A., 2000. Equatorial nutrient trapping in biogeochemical ocean models: the role of advection numerics. Global Biogeochemical Cycles 14, 655–667.

Oschlies, A., Garcon, V., 1999. An eddy-permitting coupled physical–biological model of the North Atlantic 1. Sensitivity to advection numerics and mixed layer physics. Global Biogeochemical Cycles 13, 135–160.

Peeken, I., 1997. Photosynthetic pigment fingerprints as indicators of phytoplankton biomass and development in different water masses of the Southern Ocean during austral spring. Deep-Sea Research II 44, 261–282.

Perry, M.J., Talbot, M.C., Alberte, R.S., 1981. Photoadaptation in marine phytoplankton: response of the photosynthetic unit. Marine Biology 62, 91–101.

Price, N.M., Ahner, B.A., Morel, F.M.M., 1994. The equatorial Pacific Ocean: grazer-controlled phytoplankton populations in an iron-limited ecosystem. Limnology and Oceanography 39, 520–534.

Prospero, J.M., Ginoux, P., Torres, O., Nicholson, S., Gill, T., 2002. Environmental characterization of global sources of atmospheric soil dust derived from the NIMBUS-7 TOMS absorbing aerosol product. Reviews of Geophysics, (doi: 10.1029/2000RG000095).

Robertson, J.E., Robinson, C., Turner, D.R., Holligan, P., Watson, A.J., Boyd, P., Fernandez, E., Finch, M., 1994. The impact of a coccolithophore bloom on oceanic carbon uptake in the northeast Atlantic during summer 1991. Deep-Sea Research I 41, 297–314.

Rue, E.L., Bruland, K.W., 1995. Complexation of iron(III) by natural organic ligands in the central North Pacific as determined by a new competitive ligand equilibration/adsorptive cathodic stripping voltammetric method. Marine Chemistry 50, 117–138.

Rue, E.L., Bruland, K.W., 1997. The role of organic complexation on ambient iron chemistry in the equatorial

Pacific Ocean and the response of a mesoscale iron addition experiment. Limnology and Oceanography 42, 901–910.

Sakshaug, E., Andresen, K., 1986. Effect of light regime upon growth rate and chemical composition of a clone of *Skeletonema costatum* from the Trondheimsfjord, Norway. Journal of Plankton Research 8, 619–637.

Sedwick, P.N., DiTullio, G.R., Hutchins, D.A., Boyd, P.W., Griffiths, F.B., Crossley, A.C., Trull, T.W., Queguiner, B., 1999. Limitation of algal growth by iron deficiency in the Australian subantarctic region. Geophysical Research Letters 26, 2865–2868.

Sedwick, P.N., DiTullio, G.R., Mackey, D.J., 2000. Iron and manganese in the Ross Sea, Antarctica: seasonal iron limitation in Antarctic shelf waters. Journal of Geophysical Research 105, 11321–11336.

Steinberg, D.K., Carlson, C.A., Bates, N.R., Johnson, R.J., Michaels, A.F., Knap, A.H., 2001. Overview of the US JGOFS Bermuda Atlantic Time-series Study (BATS): a decade-scale look at ocean biology and biogeochemistry. Deep-Sea Research II 48, 1405–1447.

Stuart, V., Sathyendranath, S., Platt, T., Maass, H., Irwin, B.D., 1998. Pigments and species composition of natural phytoplankton populations: effect on the absorption spectra. Journal of Plankton Research 20, 187–217.

Sunda, W.G., Huntsman, S.A., 1995. Iron uptake and growth limitation in oceanic and coastal Phytoplankton. Marine Chemistry 50, 189–206.

Takeda, S., Kamatani, A., Kawanobe, K., 1995. Effects of nitrogen and iron enrichments on phytoplankton communities in the northwestern Indian Ocean. Marine Chemistry 50, 229–241.

Tappin, A.D., Millward, G.E., Statham, P.J., Burton, J.D., Morris, A.W., 1995. Trace metals in the central and southern North Sea. Estuarine, Coastal and Shelf Science 41, 275–323.

Tarran, G.A., Burkill, P.H., Edwards, E.S., Malcolm, E., Woodward, S., 1999. Phytoplankton community structure in the Arabian Sea during and after the SW monsoon, 1994. Deep-Sea Research II 46, 655–676.

Thibault, D., Roy, S., Wong, C.S., Bishop, J.K., 1999. The downward flux of biogenic material in the NE subarctic Pacific: importance of algal sinking and mesozooplankton herbivory. Deep-Sea Research II 46, 2669–2697.

Timmermans, K.R., Gerringa, L.J.A., de Baar, H.J.W., van der Wagt, B., Veldhuis, M.J.W., de Jong, J.T.M., Croot, P.L., 2001. Growth rates of large and small Southern Ocean diatoms in relation to availability of iron in natural seawater. Limnology and Oceanography 46, 260–266.

van Leeuwe, M.A., DeBaar, H.J.W., Veldhuis, M.J.W., 1998. Pigment distribution in the Pacific region of the Southern Ocean (autumn 1995). Polar Biology 19, 348–353.

Vassiliev, I.R., Kolber, Z., Wyman, K.D., Mauzerall, D., Shukla, V.K., Falkowski, P.G., 1995. Effects of iron limitation on photosystem II composition and light utilization in *Dunaliella tertiolecta*. Plant Physiology 109, 963–972.

Wright, S.W., Thomas, D.P., Marchant, H.J., Higgins, H.W., Mackey, M.D., Mackey, D.J., 1996. Analysis of phytoplankton of the Australian sector of the southern ocean: comparisons of microscopy and size frequency data with interpretations of pigment HPLC data using the 'CHEMTAX' matrix factorization program. Marine Ecology Progress Series 144, 285–298.

Wu, J., Luther, G.W., 1996. Spatial and temporal distribution of iron in the surface water of the northwestern Atlantic Ocean. Geochmica et Cosmochimica Acta 60, 2729–2741.

Wyman, M., Fay, P., 1986. Underwater light climate and the growth and pigmentation of planktonic blue-green algae (Cyanobacteria) I. The influence of light quantity. Proceedings of the Royal Society of London 227, 367–380.

Zonneveld, C., 1997. Modeling effects of photoadaptation on the photosynthesis–irradiance curve. Journal of Theoretical Biology 186, 381–388.